Accepted version

Ciancimino A., Lanzo G., Alleanza G.A., AMOROSO S., Bardotti R., Biondi G., Cascone E., Castelli F., Di Giulio A., d'Onofrio A., Foti S., Lentini V., Madiai C., Vessia G. (2020). Dynamic characterization of fine-grained soils in Central Italy by laboratory testing. Bulletin of Earthquake Engineering, Print ISSN 1570-761X, Online ISSN 1573-1456. 18:5503–5531, doi: 10.1007/s10518-019-00611-6 [Web of Science: WOS:000565913400006, Scopus: 2-s2.0-85064595019]

Dynamic characterization of fine-grained soils in Central Italy by laboratory testing

Authors:

Andrea Ciancimino[1], Giuseppe Lanzo[2], Giorgio Andrea Alleanza[3], Sara Amoroso[4,5], Roberto Bardotti[6], Giovanni Biondi[7], Ernesto Cascone[7], Francesco Castelli[8], Anita Di Giulio[9], Anna d'Onofrio[3], Sebastiano Foti[1], Valentina Lentini[8], Claudia Madiai[6], Giovanna Vessia[5]

Affiliations:

[1] Politecnico di Torino, Italy

[2] *Sapienza* Università di Roma, Italy

[3] Università degli Studi di Napoli *Federico II*, Italy

[4] Istituto Nazionale di Geofisica e Vulcanologia, L'Aquila, Italy

[5] Università degli Studi *G. d'Annunzio*, Chieti – Pescara, Italy

[6] Università degli Studi di Firenze, Italy

[7] Università degli Studi di Messina, Italy

[8] Università degli Studi di Enna *Kore*, Italy

[9] Istituto di Geologia Ambientale e Geoingegneria, CNR, Roma, Italy

Corresponding author: andrea.ciancimino@polito.it

Abstract

The investigation of soil response to dynamic loads is necessary to predict site-specific seismic hazard. This paper presents the results of cyclic and dynamic laboratory tests carried out after the 2016-2017 Central Italy Earthquake sequence, within the framework of the seismic microzonation studies of the most damaged municipalities in the area. The database consists of 79 samples investigated by means of dynamic resonant column tests, cyclic torsional shear tests or cyclic direct simple shear tests. Results are firstly analysed in terms of field and laboratory values of small-strain shear wave velocity, highlighting the influence of the sample disturbance and of the mean effective consolidation pressure. The cyclic threshold shear strains as a function of plasticity index are then compared with findings from the published literature, and the outliers are analysed. Subsequently, the dynamic soil behaviour is investigated with reference to the small-strain damping ratio. Differences between results from different tests are analysed in the light of the loading frequencies. Finally, the database is used to develop a predictive model for soil nonlinear curves according to plasticity index, mean effective confining stress, and loading frequency. The model represents a useful tool to predict the nonlinear stress-strain behaviour of Central Italy soils, necessary to perform site-specific ground response analyses.

Keywords

Soil dynamics – Laboratory test – Shear modulus and damping ratio – Small-strain material damping – Shear wave velocity

1. Introduction

A thorough understanding of the stress-strain behaviour of soils is crucial to perform site-specific ground response analyses. Cyclic tests are carried out in laboratory to characterize the dynamic response of soils, that is necessary to predict the site response under seismic loading.

An idealized soil response under cyclic loading is illustrated in Fig. 1 in terms of hysteretic stress-strain loop, where τ and γ are the shear stress and the shear strain, respectively, while τ_c and γ_c are the cyclic shear stress amplitude and the cyclic shear strain amplitude, respectively. The reference parameters are usually the secant shear modulus (G_S) and the material damping ratio (D). At very small strains approaching zero, the secant shear modulus assumes the maximum value (G_0) (Fig. 1). The nonlinear nature of the stress-strain relationship with increasing cyclic shear strain amplitude is typically described by a normalized modulus reduction curve ($G_S/G_0 - \gamma_c$), firstly proposed by Seed and Idriss (1970). Material damping ratio represents the energy internally dissipated by the soil under cyclic loading conditions, as a consequence of friction between soil particles, nonlinear soil behaviour, and strain rate (viscous) effects. By virtue of the mathematical convenience of a viscoelastic formulation, the soil damping, at a given cyclic shear strain amplitude, is usually described with reference to the equivalent viscous damping ratio, namely the critical damping ratio of a Single-Degree-Of-Freedom system constituted by a mass connected to a linearly elastic spring and a viscous dashpot. If the system is subjected to a harmonic vibration, the stress-strain curve at resonance is described by an ellipse. The damping ratio during the loading-unloading cycles can then be evaluated as the ratio of the energy dissipated within one cycle (W_D) to the maximum elastic strain energy stored in the cycle (W_S), divided by 4π. The stress-strain loop typically described by soils subjected to cyclic shear strain (Fig. 1) is similar to the ellipse described by the SDOF system and the material damping can, therefore, be expressed in terms of the area of the loop. Nonlinearity in the stress-strain soil behaviour leads to an increase of the energy dissipation with increasing γ_c. The relationship between D and γ_c is represented by a material damping curve ($D - \gamma_c$). Both the $G_S/G_0 - \gamma_c$ curve and the $D - \gamma_c$ curve are usually represented in a semi-logarithmic plot.

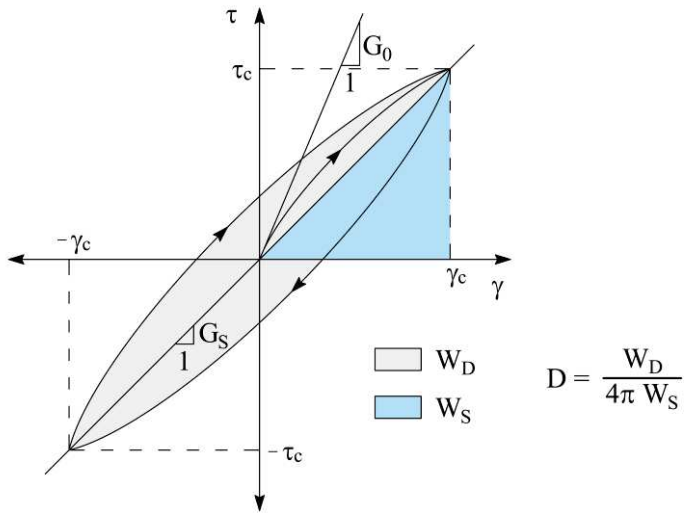

Fig. 1 Parameters describing the idealized cyclic stress-strain loop.

Silver and Seed (1971) and Youd (1972) first noticed the existence of a volumetric threshold cyclic shear strain in dry sands above which the soil experiences noticeable cyclic compression. Then, Stoll and Kald (1977) reported the presence of a cyclic threshold shear strain in a cohesionless silty soil associated with the pore water pressure build-up. The presence of the two abovementioned thresholds in sands was subsequently fully confirmed by Dobry et al. (1982) from both the experimental and the theoretical point of view. Further, the coincidence of the two thresholds for sands was also established by the Authors. The concept of threshold strains was subsequently addressed by Lo Presti (1989, 1991) who also highlighted the dependence of threshold strains in clayey soils from soil plasticity. The issue of threshold strains was then thoroughly examined by Vucetic (1992, 1994) as well as the dependency of the cyclic thresholds on the plasticity index. The Author also introduced the concept of cyclic threshold shear strains (γ_t) dividing the $G_S/G_0 - \gamma_c$ and $D - \gamma_c$ curves in three different domains of cyclic soil behaviour (i.e. very small strains, small-to-medium and medium-to-large strains).

At very small strains, below the linear threshold shear strain (γ_{tl}), the soil behaviour is practically linear and, consequently, G_S is usually approximated to a constant value (G_0). Because of this convenient approximation, from a mathematical point of view the area inside the hysteresis loop, at very small strains, is practically null and no dissipation takes place. However, the experimental evidence highlighted an amount of constant minimum energy dissipated, even in the almost linear elastic range. In this range, the energy dissipation is given mainly by friction between particles and viscosity and the soil exhibits an almost constant small-strain material damping ratio (D_{min}), although Shibuya et al. (1995) showed the influence of the shear strain rate on the latter. Between γ_{tl} and the volumetric threshold shear strain (γ_{tv}) the stress-strain relationship is nonlinear, and the hysteretic behaviour is characterized by minor changes in the microstructure. Above γ_{tv}, at medium to large strains, soils exhibit a gradual degradation behaviour, experiencing permanent changes in the microstructure and, in drained conditions, volume variation. Vucetic (1994) and more

recently Tabata and Vucetic (2010) and Mortezaie and Vucetic (2016) distinguished the amplitude below which there is practically no degradation, defined as cyclic degradation threshold shear strain (γ_{td}), and the amplitude below which there is practically no permanent cyclic pore water pressure build-up, known as cyclic pore-water pressure generation threshold shear strain (γ_{tp}). γ_{td} is typically smaller than γ_{tv} and the ratio γ_{tp}/γ_{td} varies between 1.2 and 1.6.

Over the past decades, many research efforts have been devoted to identifying the key parameters that influence the dynamic properties of soils. The main parameters are the plasticity index (PI), the effective mean confining stress (σ'_m), the loading frequency (f), the number of loading cycles (N), and the over-consolidation ratio (OCR). Kokusho et al. (1982) firstly showed the influence of the PI on the normalized modulus reduction curves of fine-grained soils. Soils characterized by high PI exhibit higher G_S/G_0 at a given γ_c amplitude. The correlations between D and PI, and G_S/G_0 and PI, at a given γ_c were subsequently presented by Dobry and Vucetic (1987), along with some indications on the influence of σ'_m on G_S/G_0 and D. Then, Vucetic and Dobry (1991) provided representative $G_S/G_0 - \gamma_c$ and $D - \gamma_c$ curves in a chart showing that PI is the most influent parameter governing the nonlinear dynamic behaviour. The effect of σ'_m was also recognized by Ishibashi and Zhang (1993) and Lanzo et al. (1997). Specifically, $G_S/G_0 - \gamma_c$ curves tend to be higher with increasing σ'_m, while lower $D - \gamma_c$ curves are expected. Nevertheless, the importance of σ'_m decreases with increasing PI (Lanzo et al., 1997). The OCR is recognized as an increasing factor of G_S/G_0, although it is considered to be a secondary factor (e.g., Kokusho et al., 1982; Vucetic and Dobry, 1991; Lanzo et al., 1997; Darendeli, 2001). The characteristics of the dynamic loading also affect the nonlinear behaviour of soils. The effect of f is recognized as an increasing factor for G_S and D (e.g., Isenhower and Stokoe, 1981; Stokoe et al., 1999; Lo Presti et al., 1997; Matešić and Vucetic, 2003). In particular, Isenhower and Stokoe (1981) first and Matešić and Vucetic (2003) later showed that G_S/G_0 increases with the average rate of shearing and its effect can be considerable, especially in the small-strain range. However, its influence is usually neglected on G_S/G_0, but it is considered relevant on D_{min} (Darendeli, 2001). The relevance of N is slightly evident at γ_c values above γ_{td} (e.g., Vucetic and Dobry, 1991; Lo Presti et al., 1997; Darendeli, 2001). However, at γ_c levels generally reached by cyclic and dynamic tests, N has a minor impact on D.

Several empirical relationships have been developed to predict the $G_S/G_0 - \gamma_c$ and $D - \gamma_c$ curves for silts and clays, according to the main parameters affecting the nonlinear behaviour. As mentioned above, Vucetic and Dobry (1991) presented the $G_S/G_0 - \gamma_c$ and $D - \gamma_c$ curves in charts as a function of the PI. Darendeli (2001), on the basis of the results of an extensive laboratory investigation, proposed a model incorporating the effect of all the key parameters. Zhang et al. (2005) developed a model including the effect of σ'_m on G_S/G_0, whose importance decreases with increasing PI. Vardanega and Bolton (2013) fitted a modified hyperbolic model to the results of 67 tests on 21 clays

and silts in which G_S/G_0 tends to be higher with increasing PI. Recently, Akeju et al. (2017) proposed a procedure based on the Bayesian approach to develop a reliable model for $G_S/G_0 - \gamma_c$ curves. The procedure is applied on results of cyclic tests performed on 26 samples of different soils, ranging from coarse sand to fine gravel. The proposed approach provides not only the optimal model parameters, but also the associated uncertainties in a rigorous manner, providing a useful tool for probabilistic analyses.

However, Kishida (2016) recently showed, through a residual analysis, that the relationships used in practice are affected by some uncertainties, depending on the combination of predictor variables adopted and on the experimental data fitted. Within this framework, the adoption of specific predictive models is essential to perform a site-specific ground response analysis in a given geological scenario.

In this paper, a database of 79 dynamic and cyclic laboratory test results on silts and clays is presented. The experimental data come from dynamic resonant column (RC) tests, cyclic torsional shear (TS) tests or cyclic double specimen direct simple shear (DSDSS) tests carried out after the 2016-2017 Central Italy Earthquake sequence, as part of the seismic microzonation studies of the most damaged municipalities in the area. A comparison between field and laboratory values of small-strain shear wave velocity (V_S) is firstly provided to show the relevance of sample disturbance and mean effective consolidation pressure. The dynamic soil behaviour is then analysed with reference to the cyclic threshold shear strains and the small-strain damping ratio. Results enlighten the peculiarities of the investigated soils compared with findings from the published literature. Moreover, the cyclic pore-water pressure generation threshold shear strain has proved to be a reliable quality index of experimental tests.

Finally, a statistical analysis of the database is performed to update the Darendeli (2001) predictive model. The updated model is able to capture the dynamic nonlinear behaviour of typical soils from the Central Italy area. However, results emphasize the shortcomings of this predictive model, specifically with reference to the prediction of the linear cyclic threshold.

2. Database

Laboratory tests were carried out within the framework of the project for the level 3 seismic microzonation of several municipalities damaged by the 2016-2017 Central Italy seismic sequence. The database includes the experimental results obtained on 79 specimens from 69 municipalities of 4 Central Italy Regions: Abruzzo, Marche, Umbria, and Lazio. The locations of the investigated sites are plotted in the map of Central Italy shown in Fig. 2. Laboratories of several universities were involved in the project, namely: the *Politecnico di Torino* (POLITO), the *Università degli Studi di Firenze* (UNIFI), the *Università degli Studi di Enna "Kore"* (UNIKORE), the *Università degli Studi di*

Messina (UNIME), the *Università degli Studi di Napoli "Federico II"* (UNINA), the *Sapienza Università di Roma* (UNIROMA1), and the *Università degli Studi "G. d'Annunzio" Chieti – Pescara* (UNICH).

The experimental data include the basic properties of the specimens and the results from RC, TS, and DSDSS tests carried out by the involved laboratories. In addition, measurements of *in-situ* shear wave velocity with depth were available from down-hole tests performed in the same boreholes from which samples were retrieved (further details on the geophysical surveys are provided in Caielli et al., 2019). A summary of the laboratory tests is given in Table 1.

Table 1 Summary of the experimental test results contained in the database.

Laboratory	Testing apparatus	Nr. of samples	Depth, z [m]	Unit weight, γ [kN/m^3]	Plasticity Index, PI [%]	Mean effective confining stress, σ'_m [kPa]
POLITO	RC/TS	12	1.6-33.8	19.0-22.0	8-36	60-350
UNIFI	RC	9	3.0-18.0	16.3-20.5	4-36	35-200
UNIKORE	RC/TS	8	5.1-20.8	15.6-21.3	0-34	65-365
UNIME	RC/TS	10	2.7-9.3	18.9-20.8	0-23	50-175
UNINA	RC/TS	21	2.2-21.3	19.3-21.6	0-42	70-440
UNIROMA1	DSDSS	19	3.0-36.0	16.5-21.0	0-37	30-200

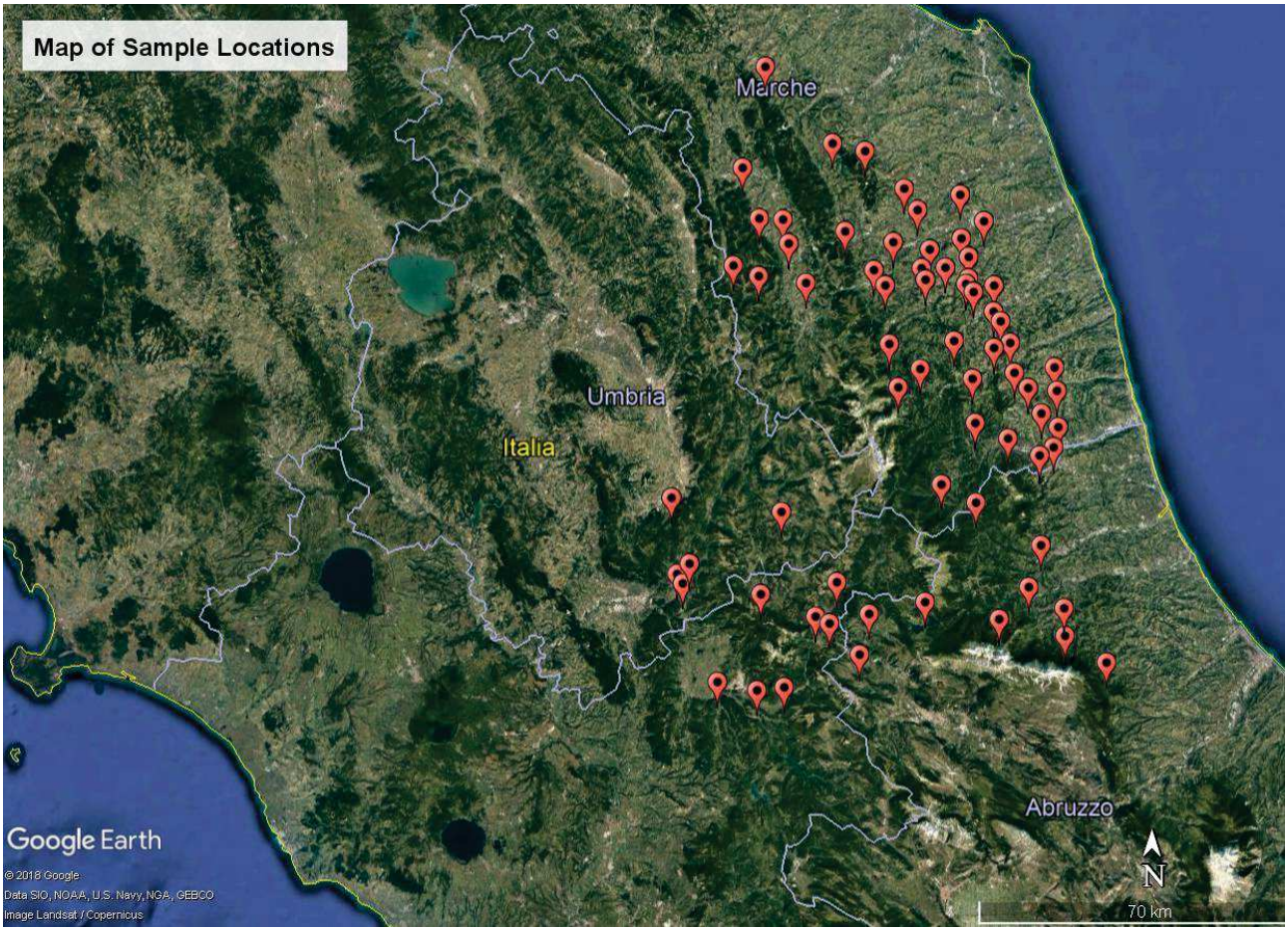

Fig. 2 Map of Central Italy showing the locations of the investigated sites (Map data: Google, SIO, NOAA, U.S. Navy, NGA, GEBCO).

Distributions of the specimens with respect to grain size distribution, PI, σ'_m, and G_0 are presented in Fig. 3. For the sake of simplicity, the classification of the samples is reported as a function of the two higher sieve fractions. The grain size distributions for all the samples studied are also reported in Fig. 4. The database mainly consists of silts with clay and silts with sand, with PI ranging from 0 to 42 %. Laboratory tests were carried out under σ'_m varying between 30 and 440 kPa, obtaining G_0 ranging from 7 to 220 MPa (the G_0 values were obtained from the first γ_c level investigated for each test, ranging from 10^{-4} to 10^{-3} %). The σ'_m values were generally defined on the basis of expected *in situ* conditions, except for some cases that will be discussed in section 4.1. Some basic properties of the tested fine-grained soils are shown in the Casagrande chart and in the activity chart of Fig. 5. According to the Unified Soil Classification System (USCS, ASTM International, 2011), the tested soils are mainly classifiable as low and normal active clays and silts of low plasticity.

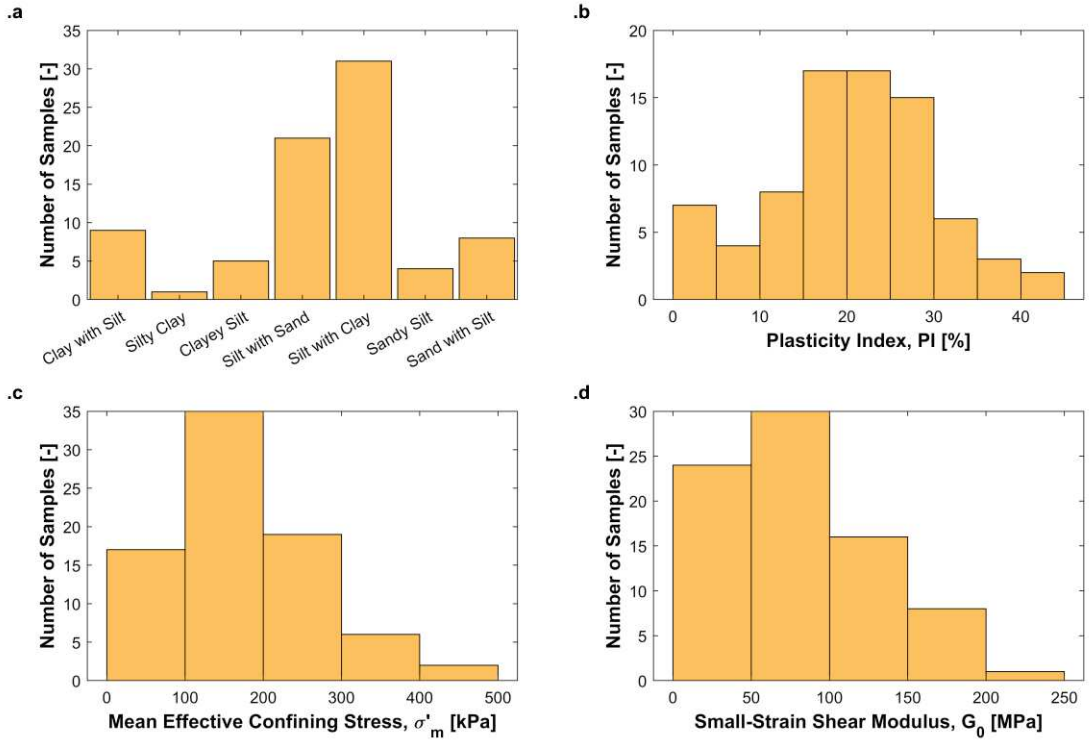

Fig. 3 Distribution of the main characteristics of the specimens: a) grain size distribution; b) plasticity index; c) testing mean effective confining stress; d) small-strain shear modulus.

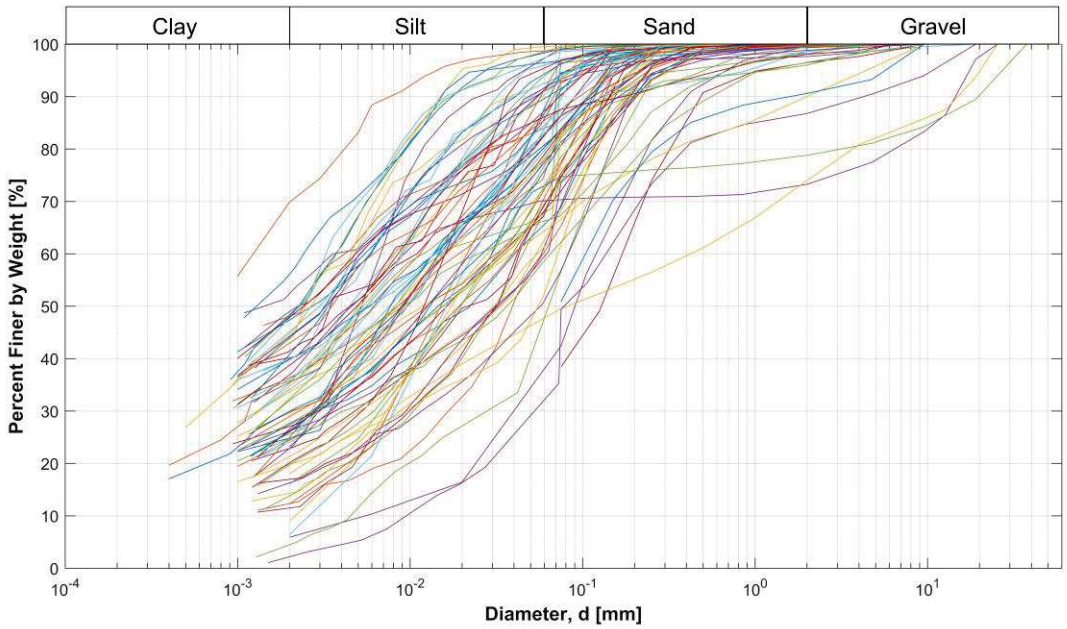

Fig. 4 Grain size distributions of the samples.

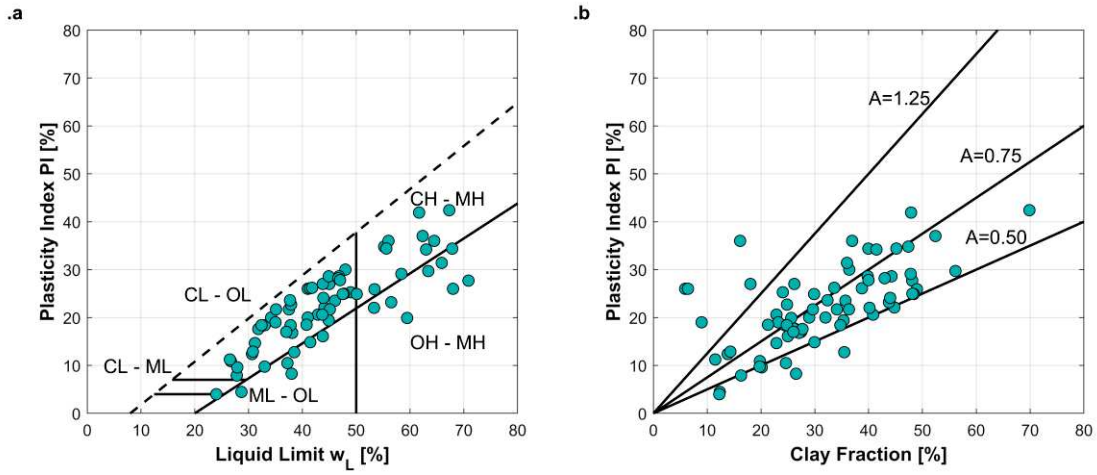

Fig. 5 Classification of the tested soils according to (a) Casagrande chart and (b) activity chart.

3. Cyclic and dynamic laboratory tests

Three different types of laboratory tests were carried out to investigate the nonlinear behaviour of soils: RC, TS, and DSDSS tests. Details about the type of test performed by each laboratory involved in the project are presented in Table 1. In total, the database consists of 9 RC tests, 51 combined RC/TS tests, and 19 DSDSS tests.

3.1. DSDSS tests

Double specimen direct simple shear tests were carried out at the Geotechnical Laboratory of the Department of Structural and Geotechnical Engineering of UNIROMA1, Faculty of Architecture. The apparatus is a simple shear device specifically designed for small-strain testing (Doroudian and Vucetic, 1995). Due to its double specimen configuration, typical frictional problems that characterize the standard direct simple shear device designed by the Norwegian Geotechnical Institute (Bjerrum and Landva, 1966) were eliminated. As consequence, the DSDSS device is

able to measure the cyclic properties of soils also at very small strains, capturing the $G_S/G_0 - \gamma_c$ and the $D - \gamma_c$ curves for a wide γ_c range (Doroudian and Vucetic, 1998). Tests are carried out under constant volume conditions and a horizontal piston is used to apply the cyclic loading. A detailed description of the apparatus available at the University of Rome can also be found in D'Elia et al. (2003).

The specimens are initially consolidated under anisotropic conditions. In this regard, it should be pointed out that the σ'_m value is estimated under the assumption of a coefficient of earth pressure at rest (K_0) of 0.5. The anisotropic σ'_m is then evaluated as: $(\sigma'_v + 2\sigma'_h)/3$. After the consolidation phase, cyclic loadings are applied with increasing cyclic shear strain amplitudes varying in the range from 10^{-4} to 7 %. The test is performed under displacement control conditions. G_S and D are directly measured from the cyclic stress-strain loop, according to the γ_c reached. For each γ_c, 10 loading cycles are applied with a loading frequency of about 0.25 Hz. No data about pore water pressure build-up are available.

As an example, Fig. 6 shows the results of the DSDSS test carried out on the Montereale specimen ($PI = 24.9$, $\sigma'_v = 250\ kPa$) in terms of stress-strain loops, for increasing γ_c values in the range 0.00044-0.11% showing the capability of the DSDSS device to investigate the small-to-medium strain range.

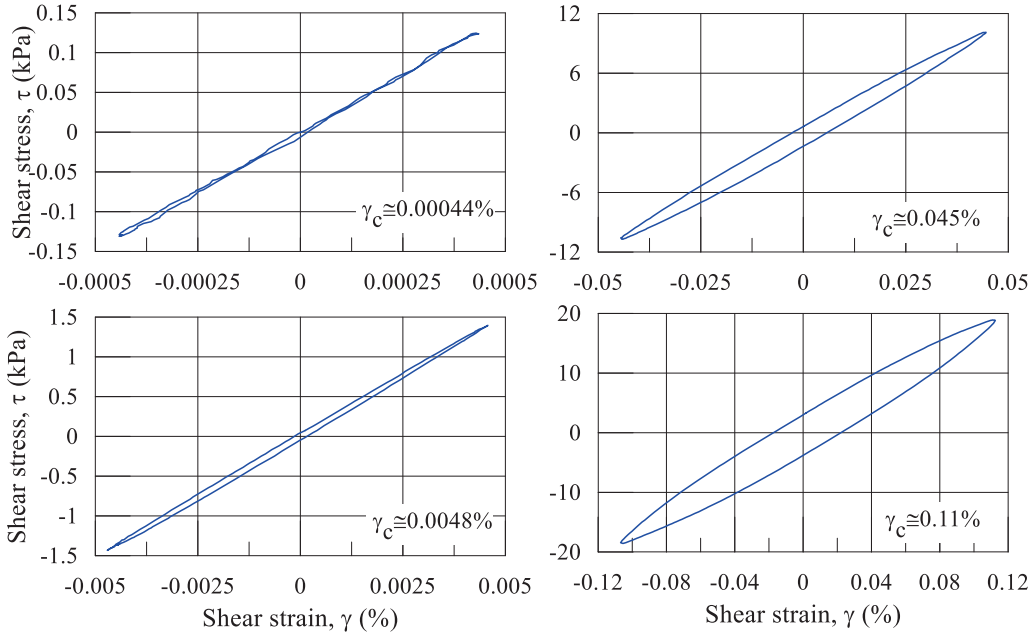

Fig. 6 Cyclic stress-strain loops obtained from the Montereale specimen ($PI = 24.9$) in DSDSS tests at $\sigma'_v = 250\ kPa$ for increasing levels of γ_c.

3.2. RC tests

Resonant column tests were carried out by the other laboratories involved in the project. The devices used are generally modified versions of the free-fixed type apparatus designed at the University of Texas at Austin and described by Isenhower (1979). The same devices were subsequently used by some of the laboratories to perform TS tests on the same specimens.

A cylindrical soil specimen is prepared and installed in a compressed air cell. The specimen, submerged by water, is then saturated through a back-pressure process and consolidated with an isotropic effective confining stress ($K_0 = 1$). After this phase, it is excited with a constant torque loading at the top free end by an electromagnetic driving system, while the bottom is fixed. The test is performed under loading control conditions and in undrained mode. The same loading torque is applied at different frequencies, while an accelerometer installed at the top cap provides a measurement of the specimen response in terms of rotation. Several cycles are applied for frequencies variable in a wide range, according to the expected first-mode resonance frequency of the specimen (f_0). Cyclic shear strain amplitude generally ranges from 10^{-5} to 0.5 %. The apparatuses are usually instrumented for pore water pressure measurements, but data are available only for 36 RC tests.

The response function of the specimen (i.e. the rotation, θ, vs frequency curve) is used to estimate f_0 as the frequency corresponding to the maximum rotation (θ_{max}). The equation of motion for torsional vibrations allows estimating the shear wave velocity (V_S):

$$\frac{I_\theta}{I_t} = \frac{2\pi f_0 H}{V_S} \tan\left(\frac{2\pi f_0 H}{V_S}\right) \quad (1)$$

where I_θ is the specimen polar moment of inertia, I_t is the driving system polar moment of inertia and H is the height of the specimen. The secant shear modulus G_S is then obtained from $G_S = \rho V_S^2$, where ρ is the soil density.

D is calculated using either the half-power bandwidth or the free-vibration decay method. The first method is based on the measurement of the width of the frequency response curve around the resonance frequency:

$$D_{hp} = \frac{f_2 - f_1}{f_0} \quad (2)$$

where f_1 and f_2 are the frequencies associated to a θ amplitude equal to $\sqrt{2}/2 \cdot \theta_{max}$. The free-vibration decay method can be alternatively used. The sample is excited initially at f_0, then the input current is switched off to perform a free-vibration test and the amplitude decay is recorded with time by the accelerometer. The peak amplitude (z_n, where n is the number of the cycle) is determined for each cycle and then the values of logarithmic decrement (δ) and material damping (D_{fd}) are computed respectively as:

$$\delta = \frac{1}{n-1} \ln\left(\frac{z_1}{z_n}\right) \quad (3)$$

$$D_{fd} \approx \frac{\delta}{2\pi} \quad (4)$$

In this study, the free-vibration method data, when available, were preferred to data from the half-power bandwidth method. Although recent studies revealed a good matching between free-vibration decay and measurements in steady-state vibration (e.g., Senetakis et al., 2015), a well-recognized source of error in RC measurements of D arises in fact

from the use of an electromagnetic driving system to provide the torsional excitation (e.g., Kim, 1991; Hwang, 1997; d'Onofrio et al., 1999; Cascante et al., 2003; Wang et al., 2003; Meng and Rix, 2003). If the input current is switched off, as in the case of the free-vibration method, the resulting material damping ratio is less affected by this bias.

In Fig. 7.a-b the results of the RC test carried out on the Acquasanta Terme specimen ($PI = 17$ %, $\sigma_m{}' = 60\ kPa$) are plotted in terms of input loading torque and output acceleration time-histories for three different frequencies. Fig. 7.c reports the output amplitude vs f curves obtained for the same specimen, for different loading torques. Finally, Fig. 7.d reports an example of the application of the free-vibration decay method for a given loading torque.

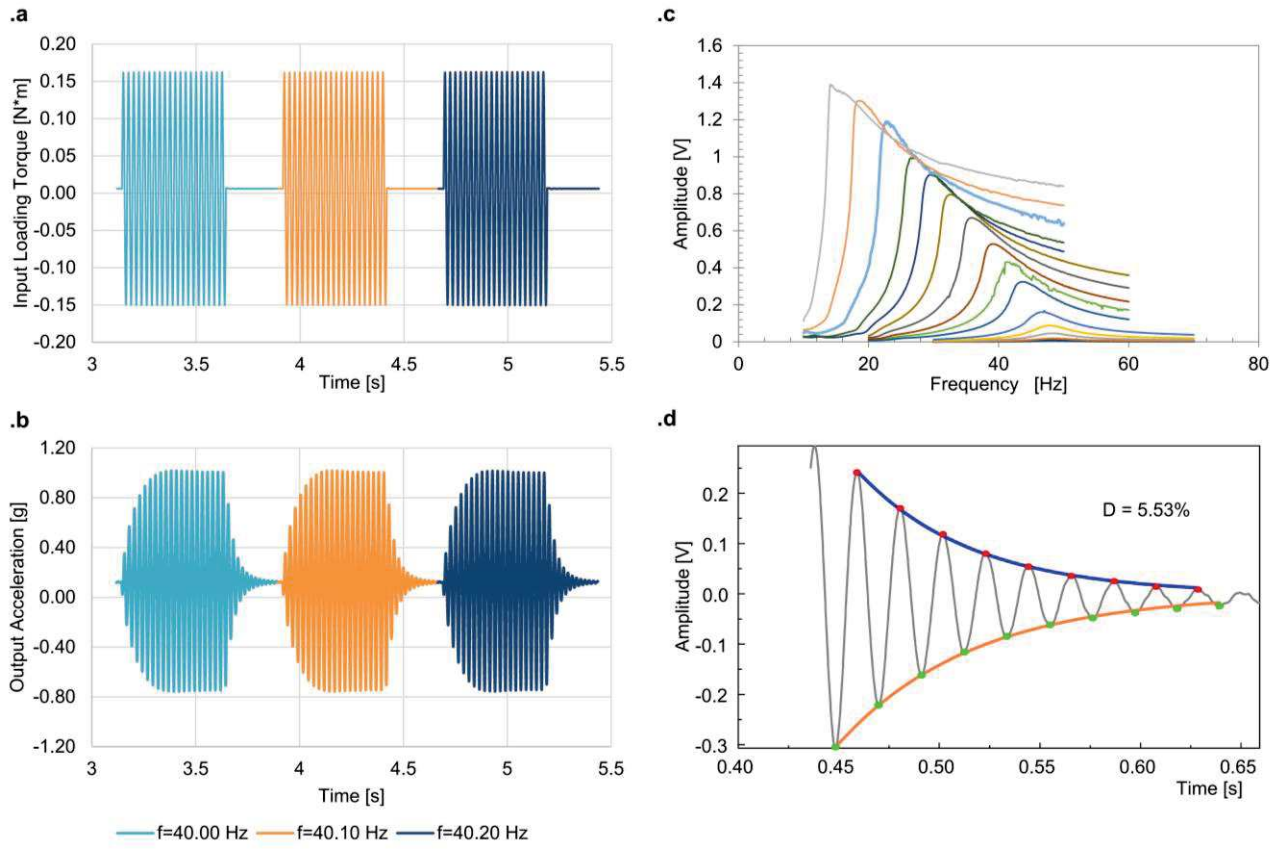

Fig. 7 Results of the RC tests carried out by POLITO on the Acquasanta Terme specimen ($PI = 17$ %) at $\sigma_m{}' = 60\ kPa$: (a) input loading torque and (b) output acceleration time-histories for three different frequencies; (c) output amplitude vs f curves; (d) free-vibration decay plot.

3.3. TS tests

Torsional shear tests are usually performed after RC tests on the same specimen and with the same device. The driving system applies a fixed number of sinusoidal cycles (5-10) at a fixed excitation frequency (0.1-0.5 Hz). The hysteretic loop can be plotted in the stress-strain plane and, for each γ_c value, G_S and D can be directly computed from the unloading-reloading loops.

In the present study, the TS tests were used mainly for comparisons against the results from RC tests in terms of $D - \gamma_c$ curves. This is because the TS tests were not carried out on all the samples and some tests were not performed at an adequate number of γ_c values to describe the nonlinear behaviour of the soil.

3.4. Results

The results of the cyclic and dynamic tests performed are here presented in terms of nonlinear variation of G_S/G_0 and D versus γ_c and, when available, pore-water pressure build-up versus γ_c.

In Fig. 8 the $G_S/G_0 - \gamma_c$ and $D - \gamma_c$ experimental results for all the specimens tested in DSDSS and RC apparatuses are shown. Data are plotted as a function of PI of the sample. A clear trend with PI is evident both for the $G_S/G_0 - \gamma_c$ data and the $D - \gamma_c$ data. In particular, soils characterized by high PI exhibit higher G_S/G_0 at a given γ_c, according to the trends defined in the previously published literature (e.g., Kokusho et al., 1982; Dobry and Vucetic, 1987; Vucetic and Dobry, 1991; Darendeli, 2001). The D curves are instead charcterized by a cross-over shear strain separating the small-strain range from the medium-to-large-strain range. At small strains, soils characterized by high PI values exhibit higher D values, while at small and medium strains smaller D values are expected for soils characterized by high PI values. Experimental data are then consistent with the trend observed by EPRI (1993), explained by Lanzo and Vucetic (1999) and confirmed also by Stokoe et al. (1995) and Stokoe et al. (1999).

However, for a given range of PI values, a higher dispersion of D is observed in comparison with the G_S/G_0 data, especially in the small-strain range. This observation will be discussed in detail in section 4.3, but this is mainly due to the influence of loading frequency and PI on D_0, and to the high variability that affects the material damping ratio at medium and large strain levels. Furthermore, another source of varibility on damping measurements is given by the internal equipment-generated damping in the RC test due to the back electro-magnetic force (e.g., Kim, 1991; Hwang, 1997; d'Onofrio et al., 1999; Cascante et al., 2003; Wang et al., 2003; Meng and Rix, 2003).

G_S/G_0 data for some high plasticity soils in Fig. 8 are approximately equal to 1 up to γ_c of 10^{-2} %. This could suggest that their behaviour is completely linear elastic in the small-strain range. However, as also discussed in the introduction, the soil behaviour is nonlinear also at very small strains and the soil linearity is just a convenient engineering approximation. In fact, if soils would behave linearly, the damping should be more or less equal to zero (because the area inside the hysteresis loop would be null), while soils exhibit small damping values even at very small strains. These discrepancies could be explained by considering the influence of the average rate of shearing on G_S/G_0. Soils tested at the same loading frequencies (as is the case of DSDSS tests and RC tests at small strains, where the resonance frequencies are approximately the same) are in fact characterized by larger strain rates with increasing γ_c values. This leads to an increase of G_S/G_0 and can result to an almost constant G_S/G_0 equal to 1 (Isenhower and Stokoe, 1981; Matešić and Vucetic, 2003).

A systematic comparison between experimental G_S/G_0 and D values obtained in the present study and values provided by the most used predictive relationships (i.e. Vucetic and Dobry, 1991; Darendeli, 2001; Vardanega and Bolton, 2013) was carried out by Ciancimino et al. (2019), revealing that experimental data are in good agreement with predictive

models in the medium to large strain range, while some discrepancies are observed in the small-strain range. In particular, only the Vucetic and Dobry (1991) curves are able to capture the experimental cyclic linear thresholds. This issue is discussed in detail in section 4.2.

Available data of pore-water pressure build-up are reported in Fig. 9 for 36 RC tests. Data are plotted both in terms of cyclic pore-water pressure (Δu) and normalized cyclic pore-water pressure ($u^* = \Delta u/\sigma'_m$) with increasing γ_c values, as a function of PI. A trend between the cyclic pore-water pressure generation threshold shear strain and the PI can be recognized. As PI increases, γ_{tp} tends also to increase, according to the results of previous studies (e.g. Vucetic, 1994; Tabata and Vucetic, 2010). It should be pointed out that pore-water pressure values reported in this paper were measured after 10 or 20 loading cycles (depending on the test) carried out at the resonance frequency. Anyway, several cycles (>1000) were applied in a wide range of frequencies preceding the resonance frequency. The reported values cannot therefore be associated to a constant number of cycles.

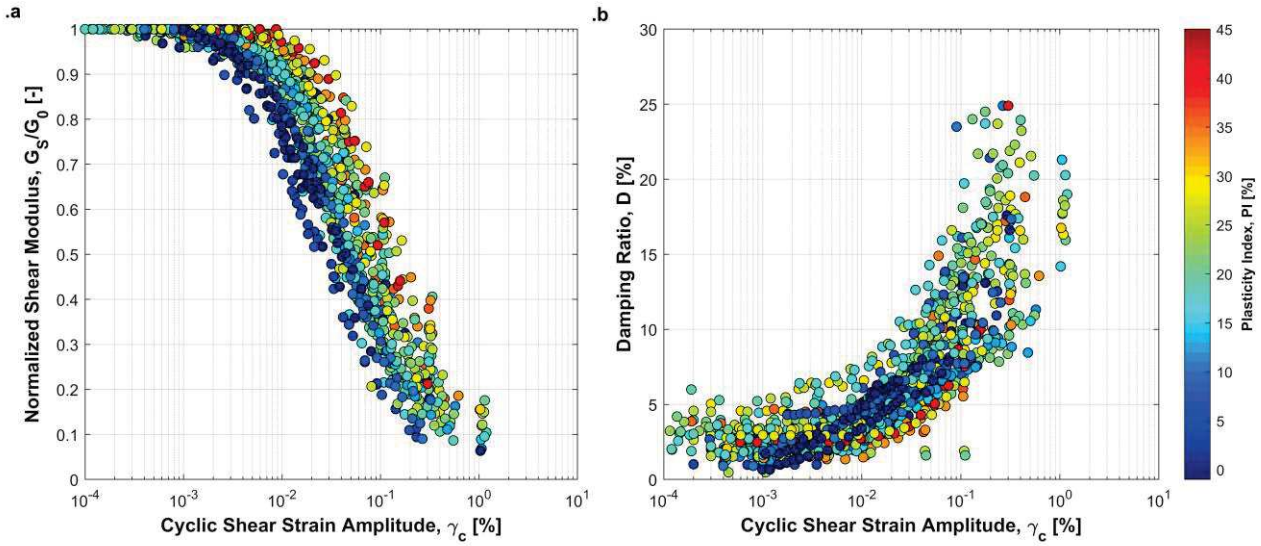

Fig. 8 Results of RC and DSDSS tests: (a) normalized shear modulus; (b) material damping ratio.

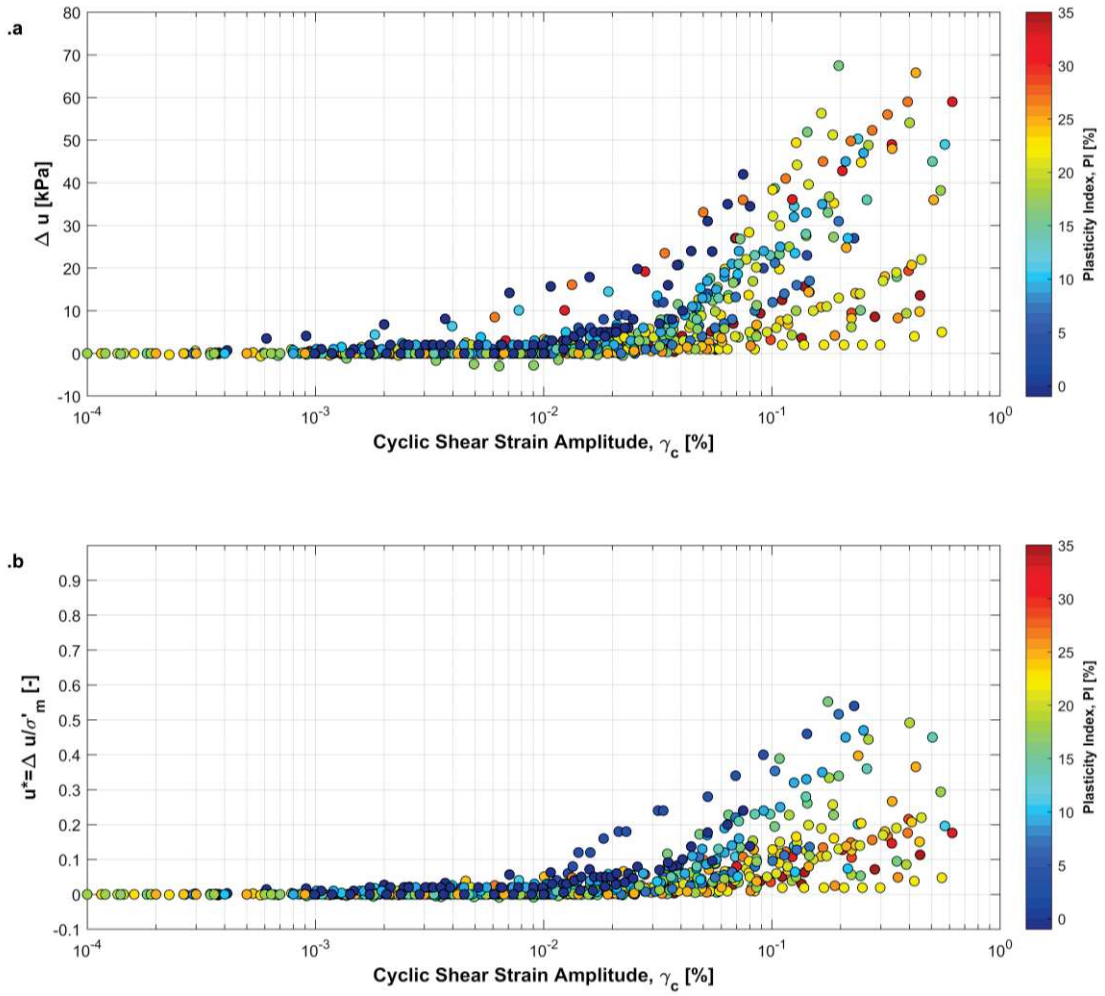

Fig. 9 Pore pressure build-up results available from 36 RC tests in terms of (a) Δu, and (b) u^*.

4. Analysis and discussion of results

An analysis of the cyclic and dynamic tests results is undertaken to highlight the peculiarities of the investigated soils. Specifically, sample disturbance effects on shear wave velocity, cyclic threshold shear strains and small-strain damping ratio are analysed with reference to findings from the published literature.

4.1. Sample disturbance effects

The evaluation of the dynamic soil properties by means of laboratory tests is constrained by sample disturbance effects. While the effects of the sampling procedures on D are not yet in-depth investigated, a lot of studies pointed out that the values of G_S (and, then, of V_S) from field and laboratory tests might be very different when compared to each other. Shear wave velocity values measured in laboratory ($V_{S,lab}$) are recognized to be from slight to considerable lower than *in situ* values ($V_{S,field}$) (Anderson and Woods, 1975). The loss in stiffness comes from irrecoverable damages at interparticle contacts, resulting in an alteration of the soil structure (Stokoe and Santamarina, 2000). As a consequence, the current state of practice is to evaluate the $G_S/G_0 - \gamma_c$ curve in laboratory and subsequently multiply the ordinate of the curve for the G_0 coming from $V_{S,field}$.

A comparison between $V_{S,field}$ from down-hole seismic tests and $V_{S,lab}$ from RC and DSDSS tests is reported in Fig. 10.a. Specifically, the variation of the laboratory-to-field V_S ratio ($V_{S,lab}/V_{S,field}$) against $V_{S,field}$ is compared to the range obtained in the framework of the ROSRINE study (Stokoe and Santamarina, 2000). Experimental data are divided in three $\sigma'_m - z$ classes according to the ranges of the effective mean confining pressure applied in the laboratory test and to the depth of sampling. The three classes are defined for different values of A in the relationship: $\sigma'_m = A \cdot z$, where σ'_m is in kPa and z is in m. The two lines that divide the plot correspond to the limit values of σ'_m that can reasonable take place in field (i.e.: saturated soils with $\gamma' = 10\ kN/m^3$, or dry soils with $\gamma = 22\ kN/m^3$). The classes are then indicative of different reconsolidation processes, as highlighted in Fig. 10.b.

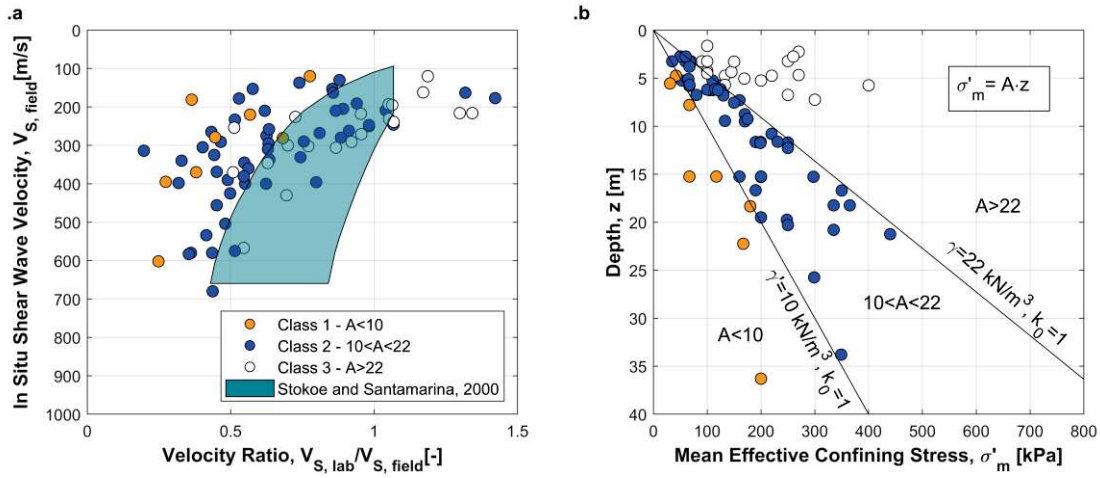

Fig. 10 Sample disturbance effects: (a) ratio of laboratory-to-field V_S against in situ values; (b) testing mean effective confining stress against depth.

The same general trend highlighted by Stokoe and Santamarina (2000) is observed in the present study. The sample disturbance effects are on average more relevant for soils characterized by higher $V_{S,field}$, but the $V_{S,lab}/V_{S,field}$ values tend to be lower as compared to the Stokoe and Santamarina (2000) range. The most pronounced effects observed in this study are probably due, for some specimens, to the sampling that was not perfectly executed and/or to a laboratory reconsolidation σ'_m lower than the confining *in situ* pressure. For highly deformable soils, the reconsolidation process induces sometimes an overestimation of $V_{S,lab}$ with respect to $V_{S,field}$, according to the testing σ'_m. Specimens in the first class ($A < 10$) were probably reconsolidated at σ'_m values lower than the confining *in situ* pressures, and then exhibit lower $V_{S,lab}/V_{S,field}$ ratio. The second class ($10 < A < 22$) includes specimens reconsolidated at a σ'_m coherent with the *in situ* stress state. Finally, specimens in the third class ($A > 22$) were reconsolidated at σ'_m values higher than the confining *in situ* pressures, involving an overestimation of $V_{S,lab}/V_{S,field}$ (ranging from 1.1 to 1.4) for the most deformable soils.

Additionally, the low $V_{S,lab}/V_{S,field}$ ratios obtained can be also due to the fact that the $V_{S,lab}$ values come from the secant shear modulus measured at the lower γ_c value investigated (i.e. G_0), the latter ranging from 10^{-4} to 10^{-3} %. For

some specimens, the G_0 values are then associated to γ_c values little beyond the elastic threshold, leading to a decrease of the $V_{S,lab}/V_{S,field}$ ratios.

4.2. Cyclic threshold shear strains

The variations of γ_{tl} and γ_{tv} with increasing PI are here analysed. Similarly to the study of Vucetic (1994), the γ_{tl} was defined as the cyclic strain corresponding to $G_S/G_0 = 0.99$. The definition of γ_{tv} was more complicated because there is no information about cyclic degradation, moreover experimental data about pore-water pressure build-up are available only for 36 samples. Vucetic (1994) however showed that before γ_{tv} is reached, shear modulus must be reduced approximately by 35 %. This is true if the γ_{tv} is defined on the basis of the pore pressure build-up, while higher values of G_S/G_0 are associated to soil degradation. The γ_{tv} was then arbitrarily defined as the cyclic shear strain amplitude corresponding to $G_S/G_0 = 0.65$ ($\gamma_{G_S/G_0=0.65}$).

A comparison between γ_{tp}, defined as the cyclic shear strain amplitude corresponding to $\Delta u/\sigma'_m = 1$ %, and γ_{tv}, as defined above, is carried out for the RC tests for which data about pore-water pressure were available, with the purpose of verifying this hypothesis (Fig. 11). The 80 % of the points (29 out of 36 points) are concentrated along the diagonal of the plot in Fig. 11, while 7 outliers fall well outside the range. While for the points along the diagonal a clear trend between γ_{tp} and PI can be recognized, the same cannot be said for the outliers. These are then analysed aiming at identifying the causes of these differences. Fig. 12 shows the results of the cyclic tests carried out on the outliers in terms of $G_S/G_0 - \gamma_c$ and $D - \gamma_c$ curves and of normalized cyclic pore-water pressure. The plot highlights an excessive G_S/G_0 decay and a rapid increase of D already in the small-strain range. In turn, a pronounced pore water pressure build-up can be identified from the first γ_c levels. Looking at the main characteristics of the outliers (Table 2), it is evident that, first of all, γ_{tp} values (ranging from 0.0005 to 0.007 %) are totally out of the expected range of values (for example Mortezaie and Vucetic, 2016 identified γ_{tp} values which range from 0.014 to 0.034 % for two reconstituted clays). These low γ_{tp} values may be partially due to excessive sample disturbance effects that destroyed the soils structure, given the low $V_{S,lab}/V_{S,field}$ observed, less than 0.6 for 4 outliers. Anyway, the issue was not yet completely solved, further analyses are then needed to define the possible underlying causes. On the contrary, γ_{tl} values of the outliers are higher than the expected values. For 6 outliers γ_{tl} is slightly less than γ_{tp}, while, absurdly, for 1 of the samples γ_{tl} is higher than γ_{tp}. This is probably due to the fact that the first investigated γ_c levels are too high relative to the low γ_{tl} values of the disturbed samples. As a consequence, the G_S/G_0 curves were erroneously normalized to G_S values not corresponding to G_0 and then γ_{tl} were not correctly evaluated.

In light of the considerations above, it was decided to remove the experimental data referred to the 7 outliers. The following analyses are therefore conducted on a subset of 72 experimental tests.

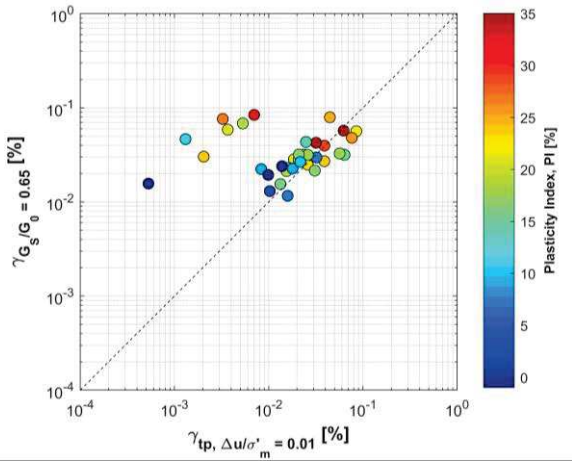

Fig. 11 Comparison between γ_{tp} and the cyclic strain corresponding to $G_S/G_0 = 0.65$ (the 7 outliers are the points above the diagonal).

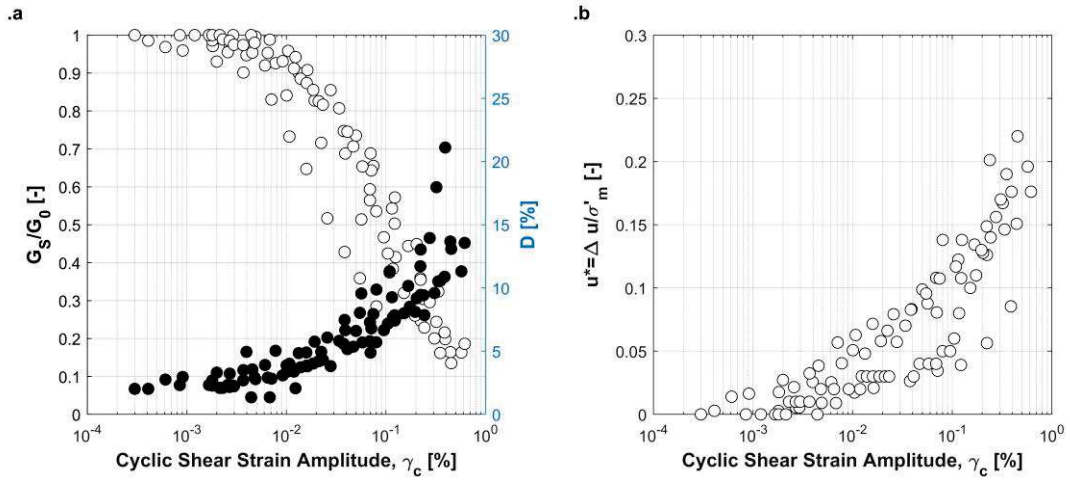

Fig. 12 Results of cyclic tests carried out on the 7 outliers: (a) normalized shear modulus (empty circles) and material damping ratio (filled circles); (b) normalized cyclic pore-water pressure.

Table 2 Summary of the experimental RC test results carried out on the 7 outliers.

Depth, z [m]	Plasticity Index, PI [%]	Mean effective confining stress, σ'_m [kPa]	Linear threshold shear strain, γ_{tl} [%]	Pore-water pressure threshold shear strain, γ_{tp} [%]	$V_{S,lab}/V_{S,field}$ [-]
11.7	12	250	0.0011	0.0013	0.44
18.3	28	335	0.0016	0.0033	0.31
5.1	25	65	0.0018	0.0020	0.32
6.3	20	110	0.0055	0.0053	0.85
20.8	34	335	0.0063	0.0070	0.57
6.2	22	100	0.0023	0.0037	0.85
12.3	0	250	0.0004	0.0005	0.56

Once conventionally defined the cyclic thresholds for all the samples, these were compared, as a function of PI, to the trends defined by Vucetic (1994) and to the thresholds implicitly assumed by the Darendeli (2001) model. Fig. 13.a shows a good agreement between experimental data from this study and Vucetic (1994) results both for γ_{tl} and γ_{tv}. On the contrary, the model proposed by Darendeli (2001) shows an underestimation of both thresholds. In particular, the γ_{tl} trends (plotted as a function of σ'_m) are far below the experimental results, especially for high PI values. As a matter of

fact, in the Darendeli (2001) database the soils with high plasticity are not well represented considering that only 10 samples with $PI > 30\%$ are present as compared to the 106 samples of the whole database. The model seems therefore not entirely adequate to describe the nonlinear response of the investigated soils. In Fig. 13.b the γ_t box plots for three different classes of PI (i.e. $0\ \% \leq PI < 15\ \%$, $15\ \% \leq PI < 30\ \%$, and $30\ \% \leq PI < 45\ \%$) are reported. The variability of γ_{tl} appears to increase with increasing PI, while for γ_{tv} no significant changes are detected. As γ_{tl} mostly defines the shape of the $G_S/G_0 - \gamma_c$ curve, higher uncertainties on the prediction of the normalized shear modulus are expected for soils with high PI values.

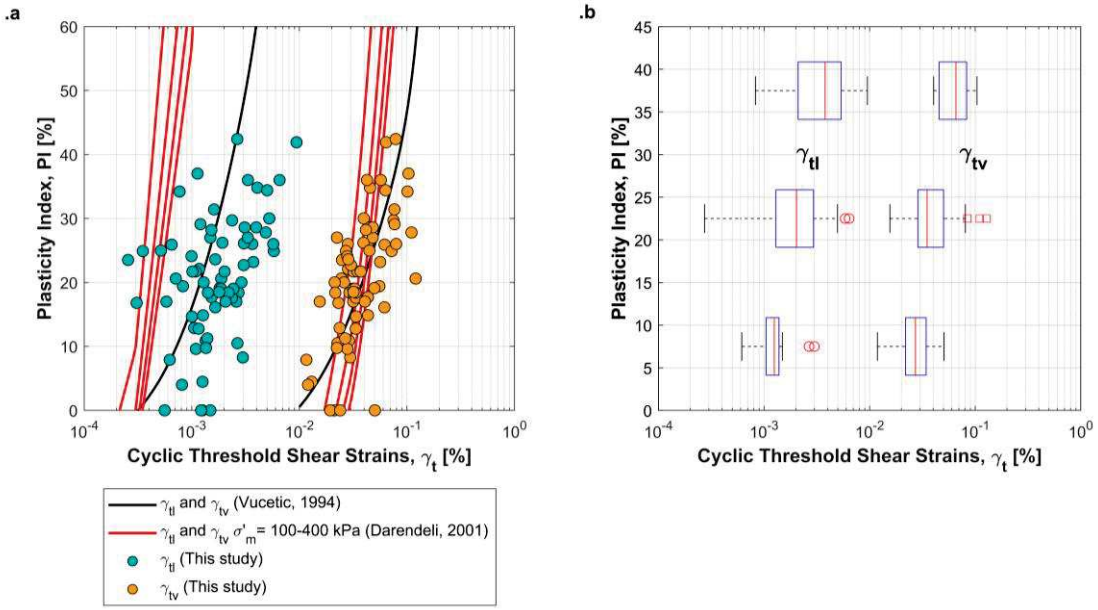

Fig. 13 Cyclic threshold shear strains against PI: (a) comparison between experimental data from this study and previous studies; (b) box plot of the experimental data.

4.3. Small-strain damping ratio

The D_{min} of soils was investigated in light of the cyclic and dynamic tests results. A statistical analysis of the RC and DSDSS experimental data was performed with the objective to study the main parameters affecting D_{min}. Following the methodology proposed by Darendeli (2001), small-strain trends in material damping can be accounted for by modelling separately the influence of PI, σ'_m, and f. No information was available about OCR, so given its minor impact it was neglected. The following relationship to predict D_{min} was calibrated on the experimental data coming from the RC and the DSDSS tests (modified from Darendeli, 2001):

$$D_{min} = (\varphi_1 + \varphi_2 \cdot PI) \cdot {\sigma'_m}^{\varphi_3} \cdot [1 + \varphi_4 \cdot \ln(f)] \quad (5)$$

According to the Darendeli (2001) formulation, PI is expressed in percentage, σ'_m is in atm, and f is in Hz. The model parameters are: $\varphi_1 = 1.2808$, $\varphi_2 = 0.0361$, $\varphi_3 = -0.2740$, and $\varphi_4 = 0.1340$. Measured and predicted D_{min} values are compared in Fig. 14. With the exception of few cases, the comparison shows a good agreement between experimental and calculated data, without highlighting clear residual trends.

The D_{min} increases with PI and f and it tends to decrease with σ'_m, consistently with the available literature; however D_{min} values predicted by Eq. (5) are significantly higher in comparison with values usually predicted by means of the most used predictive models.

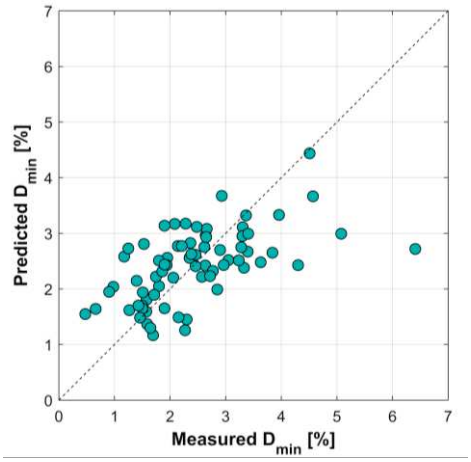

Fig. 14 Comparison between measured and predicted D_{min}.

The effectiveness of the proposed correlation was subsequently validated using the TS results, not included in the statistical analysis. In Fig. 15.a values of D_{min} resulting from TS and RC tests carried out on the same specimens are compared. Experimental data fall well below the diagonal, revealing an overestimation of the D_{min} obtained from RC tests. These differences can be attributed to the different loading frequencies applied during the tests. In fact, it is well-known that the small-strain energy dissipation, given mainly by friction between particles and viscosity, is highly influenced by the excitation frequency. For frequencies lower than 1 Hz a slight underestimation of D_{min} is expected, while for frequencies from 1 to about 100 Hz the value of D_{min} rapidly increases (e.g., Lanzo et al., 1999; Stokoe et al., 1999; Stokoe and Santamarina, 2000). The predictive relationship was then used to normalize the D_{min} values obtained from RC and TS tests to a loading frequency of 1 Hz. The normalization process was implemented by dividing the measured D_{min} by a factor equal to $[1 + \varphi_4 \cdot \ln(f)]$. The value of f is constant and equal to 0.1 or 0.5 Hz (depending on the laboratory where the tests were carried out) for the TS tests, while it is equal to the resonance frequency associated to the first γ_c level for the RC tests. The comparison shows that the differences between TS and RC results are significantly reduced applying the proposed normalization (Fig. 15.b).

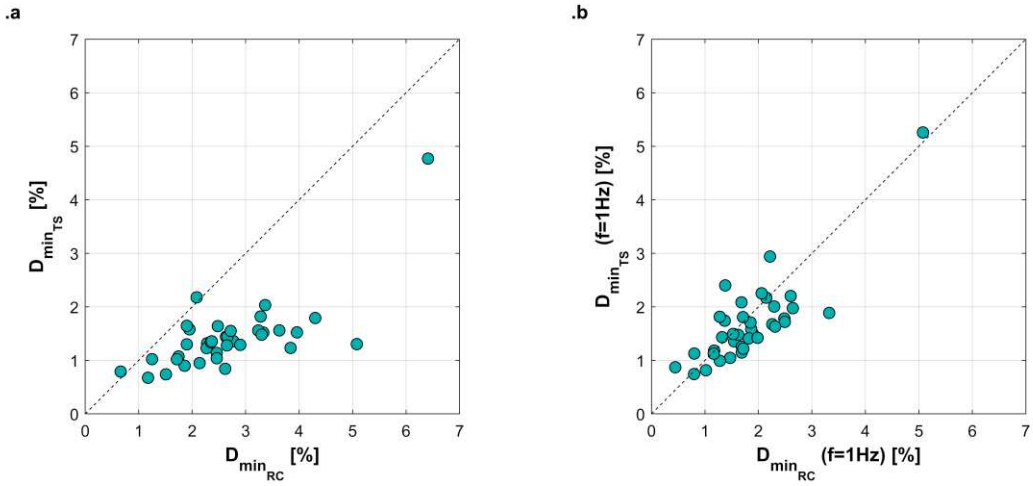

Fig. 15 Comparison between the values of D_{min} resulting from RC and TS tests without (a) or accounting for (b) the frequency normalization.

5. Predictive Model

A statistical analysis of the reliable laboratory test data was carried out to provide a tool for estimating the $G_S/G_0 - \gamma_c$ and $D - \gamma_c$ curves for the typical Central Italy soils. The analysis is based on the framework defined by Darendeli (2001) to represent the nonlinear curves of fine-grained soils. The predictive model can then be seen as an adjusted version for Central Italy soils.

5.1. G_S/G_0 and D relationships

The nonlinear stress-strain relationship is described using a modified version of the hyperbolic model proposed by Hardin and Drnevich (1972). The modified version introduces a curvature coefficient in the $G_S/G_0 - \gamma_c$ relationship to improve the fitting of the curve to experimental data. The relationship assumes the following functional form (Stokoe et al., 1999):

$$G_S/G_0 = \frac{1}{1 + \left(\frac{\gamma_c}{\gamma_r}\right)^a} \quad (6)$$

where a is the curvature parameter and γ_r is the reference strain corresponding to the cyclic shear strain amplitude when $G_S/G_0 = 0.5$.

While a is poorly correlated to soil type and loading conditions, γ_r depends on PI, σ'_m, and, to a less extent, on OCR. Neglecting the contribution of the OCR, the two parameters can be evaluated as follows (modified from Darendeli, 2001):

$$a = \varphi_5 \quad (7)$$

$$\gamma_r = (\varphi_6 + \varphi_7 \cdot PI) \cdot {\sigma'_m}^{\varphi_8} \quad (8)$$

where again PI is expressed in percentage and σ'_m in atm.

The $D-\gamma_c$ curve can be modelled expressing D as a function of G_S/G_0. This approach provides a better estimation of D, which is usually affected by a higher variability respect to G_S/G_0. In this regard Darendeli (2001) suggested to model the material damping curves assuming the Masing (1926) criteria and fitting the experimental data by means of an adjusting function (F). The general formulation of D assumes then the following functional form (Darendeli, 2001):

$$D = F \cdot D_{masing} + D_{min} \quad (9)$$

where D_{min} can be evaluated by means of Eq. (5), while D_{masing} and F can be evaluated through the following equations (from Darendeli, 2001):

$$D_{masing} = c_1 D_{masing,a=1.0} + c_2 D_{masing,a=1.0}^2 + c_3 D_{masing,a=1.0}^3 \quad (10)$$

$$D_{masing,a=1.0}(\%) = \frac{100}{\pi}\left[4 \cdot \frac{\gamma_c - \gamma_r \ln\left(\frac{\gamma_c+\gamma_r}{\gamma_r}\right)}{\frac{{\gamma_c}^2}{\gamma_c+\gamma_r}} - 2\right] \quad (11)$$

$$c_1 = -1.1143a^2 + 1.8618a + 0.2523 \quad (12)$$

$$c_2 = 0.0805a^2 - 0.0710a - 0.0095 \quad (13)$$

$$c_3 = -0.0005a^2 + 0.0002a + 0.0003 \quad (14)$$

$$F = b \cdot \left(\frac{G_S}{G_0}\right)^{0.1} \quad (15)$$

where b is the scaling coefficient. The value of b tends to slightly decrease with the number of cycles increasing (e.g., Stokoe et al. 1999; Darendeli, 2001). This trend is however negligible if compared to the uncertanties affecting nonlinear predictive models. For the sake of simplicity, the dependance of the number of cycles was here neglected and b was defined as a constant value:

$$b = \varphi_9 \quad (16)$$

After the calibration of the model parameters (from φ_1 to φ_9) the nonlinear soil behaviour can be predicted by means of Eqs. from (5) to (16).

5.2. Calibration procedure

A two-step procedure was followed to identify the model parameters. The process was initialized calibrating separately the $G_S/G_0-\gamma_c$ and $D-\gamma_c$ curves. Afterwards, the fitting parameters were updated aiming at minimizing the total error between the target and the model curves. This procedure is essential to calibrate simultaneously the parameters that define the model, given the dependence of the $D-\gamma_c$ relationship on the $G_S/G_0-\gamma_c$ values.

The first step was carried out in the following way:

1. a nonlinear least squares regression was initially performed to calibrate the independent parameters related to G_S/G_0 (from φ_5 to φ_8) and D_{min} (from φ_1 to φ_4). The values suggested by Darendeli (2001) were used to initialize the regression;
2. the D_{masing} and the predicted G_S/G_0 were calculated;
3. a nonlinear least squares regression was performed to calibrate the scaling parameter φ_9 aiming at minimizing the difference between the predicted and the experimental hysteretic damping. The value suggested by Darendeli (2001) was used to initialize the regression.

With respect to the last point, the hysteretic damping was evaluated by removing the D_{min} from the total D.

As pointed out by Zhang et al. (2005), from a mathematical point of view subtracting a constant value of D_{min} from RC data is not completely correct. In fact, during the RC test, the f_0 decreases with increasing γ_c, because of the decay of G_S. As a consequence, the rate of the damping calculated by means of Eq. (5), tends to decrease. The experimental D_{min}, usually defined at the first γ_c amplitude, is then not consistent with the lower f_0 applied at higher γ_c values. To overcome this problem, the experimental D_{min} coming from the first γ_c level of RC tests is initially normalized to $f = 1\,Hz$ (following the procedure defined in section 4.3) and multiplied by a factor $[1 + \varphi_4 \cdot \ln(f)]$, according to the different testing f for each γ_c level. Then the corrected D_{min} is subtracted by the correspondent D. Fig. 16 shows an example of the application of the procedure for the Massa Fermana BH1S1 sample. Fig. 16.a reports the comparison between RC and TS results in terms of D, while Fig. 16.b reports the normalized data. A good overlapping is evident between the two curves after the D_{min} normalization.

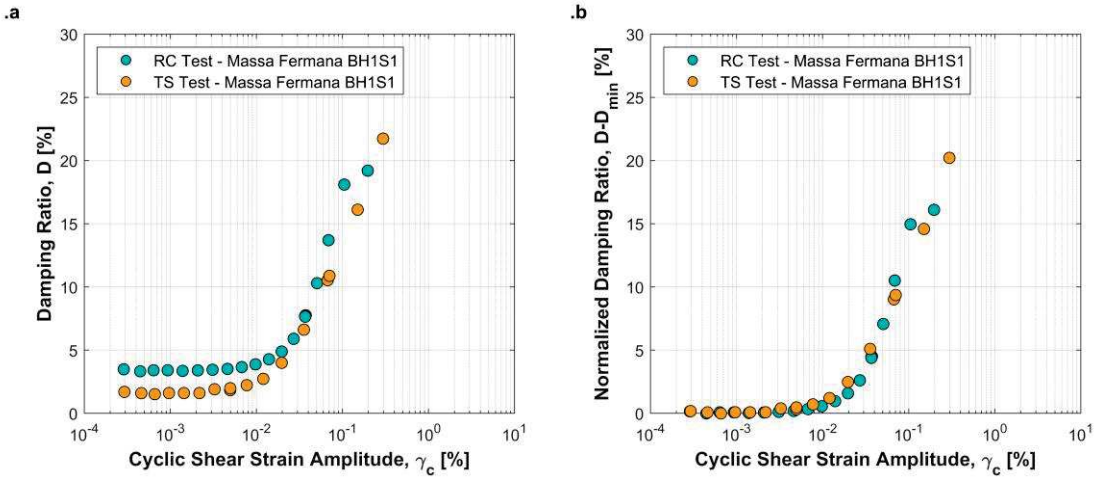

Fig. 16 Example of the D_{min} normalization process: (a) comparison between RC and TC results; (b) comparison between RC and TC results normalized to D_{min} according to the loading frequency.

The second step consists in calibrating simultaneously the G_S/G_0 and D model parameters. To address this task was necessary to define a single global error (ε) between the target and the model $G_S/G_0 - \gamma_c$ and $D - \gamma_c$ curves. For each test, ε was defined following the procedure suggested by Stewart and Hashash (reported in Stewart, 2008):

$$\varepsilon = \sqrt{(w_{G_S/G_0} \cdot \bar{\varepsilon}_{G_S/G_0})^2 + (w_D \cdot \bar{\varepsilon}_D)^2} \quad (17)$$

where $\bar{\varepsilon}_{G_S/G_0}$ and $\bar{\varepsilon}_D$ represent the mean error for the fitting of the $G/G_0 - \gamma_c$ and $D - \gamma_c$ curves respectively (with D expressed in dimensionless units). The weight factors, for a simultaneous fitting of G_S/G_0 and D, are defined by the following relationships (from Stewart, 2008):

$$w_{G_S/G_0}{}^2 + w_D{}^2 = 1 \quad (18)$$

$$w_{G_S/G_0}/w_D = \begin{cases} 1 & D_{max} > 0.25 \\ 1 + \dfrac{0.25 - D_{max}}{0.15} & 0.1 < D_{max} < 0.25 \\ 2 & D_{max} < 0.10 \end{cases} \quad (19)$$

where D_{max} is the maximum D reached for each test. A new nonlinear least squares regression was then performed aiming at minimizing the total error for each test. The model parameters defined at the first step were used to initialize the regression.

5.3. Calibration results

Results of the calibration process are reported in Table 3 in terms of the coefficients for Eqs. from (5) to (16). Measured and predicted values of G_S/G_0 and D are compared in Fig. 17.a and Fig. 18.a. The diagonal line represents the perfect fitting of the proposed equations to the experimental data (predicted values equal to measured values). Fig. 17.b and Fig. 18.b report the residuals of the predicted values against the measured values. Some discrepancies are observed. The model is not able to properly capture the γ_{tl} amplitudes observed for the experimental data. This is probably given, first of all, by the dependence of the $D - \gamma_c$ curves on the $G_S/G_0 - \gamma_c$ curves. In spite of the scaling and shifting procedure of the $D - \gamma_c$ curves, the application of the Masing (1926) criteria involves lower γ_{tl} in order to obtain simultaneously a good agreement between measured and predicted G_S/G_0 and D values. Moreover, the presence of only one curvature parameter in the G_S/G_0 relationship requires the use of a lower γ_{tl} to avoid an excessive G_S/G_0 decay at high strains. This also results in too low D values predicted at high strains.

The overall goodness-of-fit of the model was assessed through the adjusted R-squared (R^2_{adj}), computed as follows:

$$R^2_{adj} = 1 - \frac{n-1}{n-p-1} \cdot \left[\sum_{i=1}^{n} \left(Y_i - \hat{Y}_i\right)^2 / \sum_{i=1}^{n} (Y_i - \bar{Y})^2 \right] \quad (20)$$

where Y_i and $\hat{Y}_i$ are respectively the observed and predicted values of the dependent variable (i.e., G_S/G_0 or D) for the $i-th$ observation ($i = 1,2 \ldots n$), $\bar{Y}$ is the observed mean value, and p is the number of model predictors. The R^2_{adj} gives an idea of how much the predictive model explains the variance in the data, taking into account the number of explanatory variables considered. The calculated R^2_{adj} are equal to 0.943 and 0.777, respectively for G_S/G_0 and D.

These values of R^2_{adj} show the efficiency of the predictive model to capture the nonlinear behaviour of the investigated soils, in particular as regards the $G_S/G_0 - \gamma_c$ curves. The relatively lower value obtained for the $D - \gamma_c$ curves reflects the high variability that affects the soil damping ratio at medium and large strain levels. Anyway, the plots of Fig. 18 show a good global fit of the model with the experimental data. Model uncertainties associated to the proposed predictive relationships are discussed later in the paper.

Table 3 Model parameters calibrated on the RC and TS tests results.

Parameter	Mean value
φ_1	1.2808
φ_2	0.0361
φ_3	-0.2740
φ_4	0.1340
φ_5	0.9640
φ_6	0.0331
φ_7	0.0014
φ_8	0.1254
φ_9	0.5062

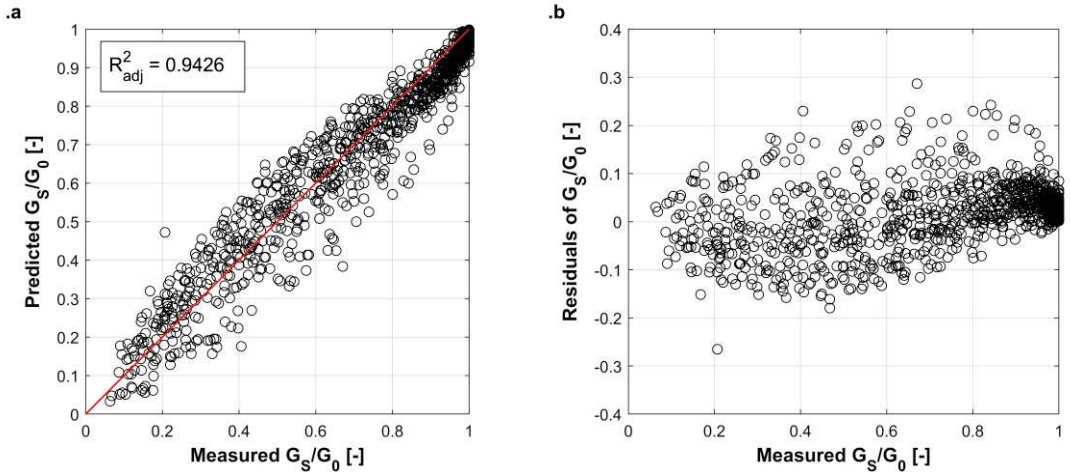

Fig. 17 Calibration process results: (a) comparison of measured and predicted G_S/G_0; (b) residuals of G_S/G_0 against measured values.

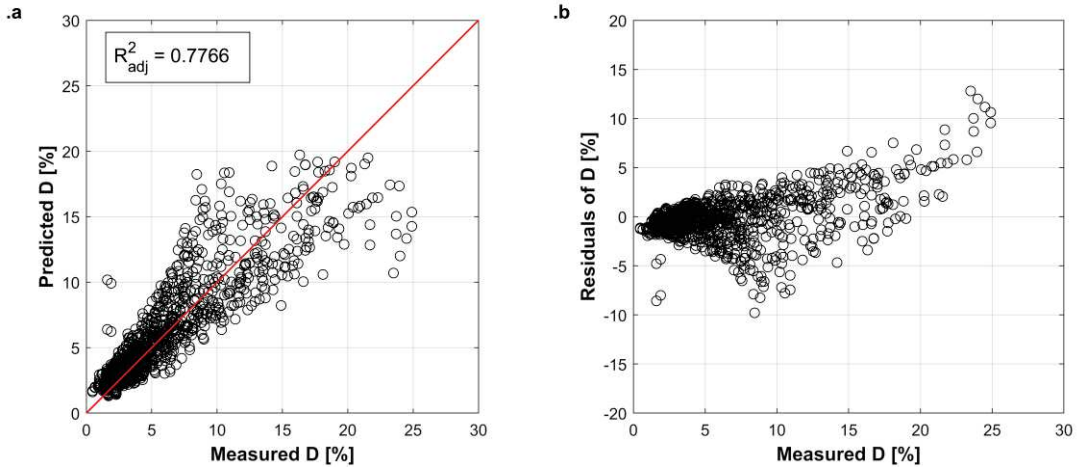

Fig. 18 Calibration process results: (a) comparison of measured and predicted D; (b) residuals of D against measured values.

The G_S/G_0 and D curves obtained herein are compared in Fig. 19 with the curves proposed by Darendeli (2001) for $PI = 0 - 45$ % (Fig. 19.a) and $\sigma'_m = 50 - 450\ kPa$ (Fig. 19.b) at f = 1 Hz. The values of N and OCR for the Darendeli relationships are assumed equal to 10 and 1, respectively. The calibrated family of curves follows the same overall trends of the Darendeli (2001) curves but some major differences can be observed, in particular for the small-strain damping. Firstly, the broader range showed in Fig. 19.a highlights a higher dependency of G_S/G_0 on PI. On the contrary, a narrower range of G_S/G_0 and D is observed with increasing σ'_m (Fig. 19.b), suggesting that the effect of σ'_m on Central Italy soils is not significant as previously thought. Finally, the mean values of D_{min} expected from the proposed model are much higher in comparison with the values predicted by applying the Darendeli (2001) relationships, especially with increasing PI and decreasing σ'_m. Although these differences can strongly influence the outcomes of site response analyses, the model reflects the high D_{min} values obtained from the experimental tests (Fig. 14). Moreover, it should be noted that laboratory measurements of D_{min} usually provide smaller values compared to the experimental evidence from downhole arrays. Larger amounts of energy loss are in fact observed also at low strain levels (Régnier et al., 2018) due mainly to the wave scattering, especially in presence of strong impedance contrasts (e.g., Stewart et al., 2014; Zalachoris and Rathje, 2015). The high D_{min} values provided by the model can then partially counteract the differences between the *in situ* and the laboratory values.

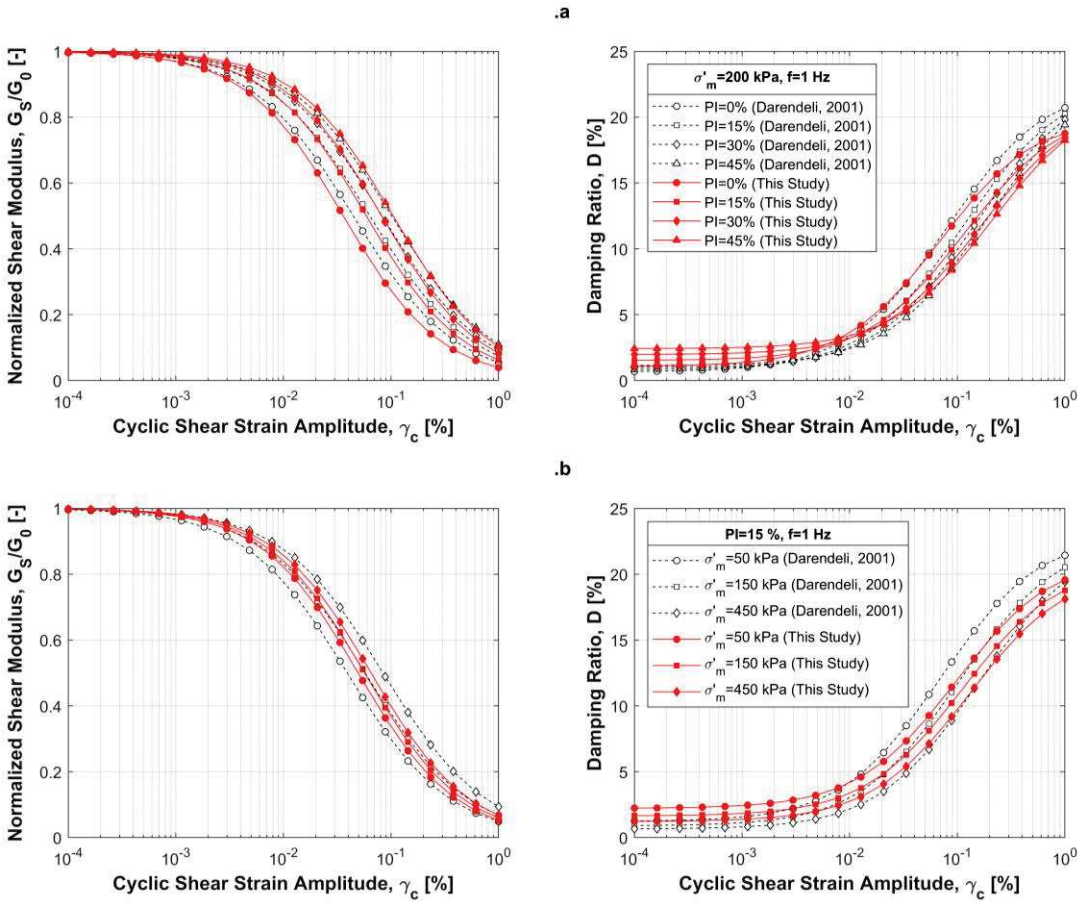

Fig. 19 Comparison of calibrated G/G_0 and D curves with curves by Darendeli (2001): (a) curves for $\sigma'_m = 200\ kPa$ and PI ranging from 0 % to 45 %; (b) curves for $PI = 15$ % and σ'_m ranging from 50 kPa to 450 kPa.

5.4. Model uncertainties

The predictive relationships proposed in this paper represent the average nonlinear response of the investigated soils. Anyway, as can be seen by Fig. 17 and Fig. 18, there are some discrepancies between experimental data and recommended curves. These discrepancies mainly depend on two different sources: the modelled variability, deriving from the physical phenomenon, and the uncertainty in the values of model parameters. As pointed out by Darendeli (2001), the second source of uncertainties is negligible when compared to the aleatory uncertainty of the measurements. As a consequence, mean values and standard deviations can be evaluated ignoring the uncertainty regarding the model parameters. In this framework, an estimation of the standard deviation was obtained calibrating the following relationships (modified from Darendeli, 2001):

$$\sigma_{G_S/G_0} = e^{-17.6673} + \sqrt{\frac{0.25}{e^{3.3747}} - \frac{(G_S/G_0 - 0.5)^2}{e^{3.3747}}} \quad (21)$$

$$\sigma_D = e^{-0.6243} + e^{-1.5001} \cdot D \quad (22)$$

where G_S/G_0 and D are the predicted mean values. The equation for σ_{G_S/G_0} has the same functional form of the relationship proposed by Darendeli (2001), while the second equation is a modified version in which σ_D depends on D rather than $\sqrt{D}$.

The model parameters were calibrated by fitting the standard deviation equations to the residuals computed over the measured values. As an example, the mean values along with the associated variability of the G_S/G_0 and D curves are represented in Fig. 20 for $PI = 15$ % and $\sigma'_m = 200\ kPa$. Experimental data in the range of $10\% < PI < 20\%$ and $100\ kPa < \sigma'_m < 300\ kPa$ are also plotted in Fig. 20. The comparison shows a good agreement between the predictive model and the experimental data, which are concentrated inside the range defined by the standard deviation.

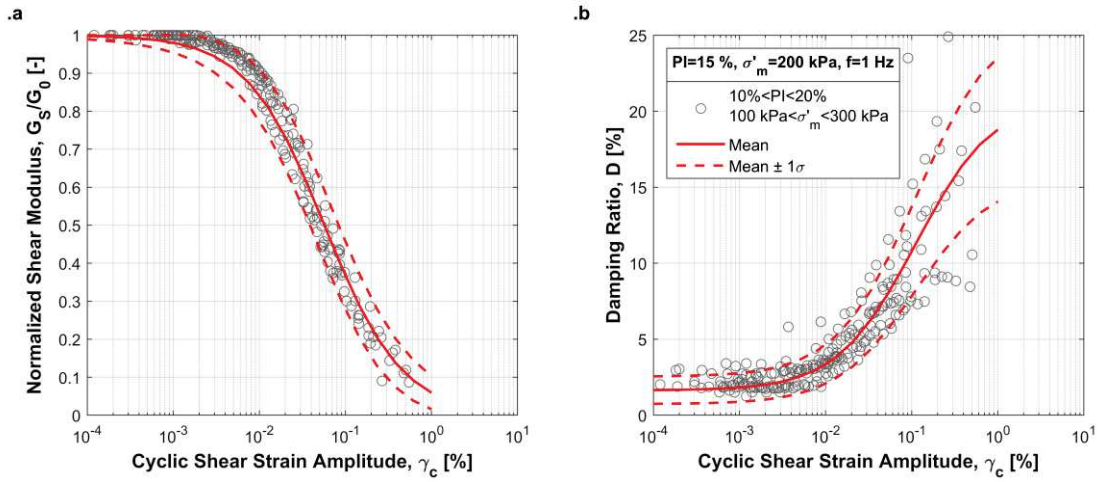

Fig. 20 Recommended mean $\pm 1\sigma$ (a) G_S/G_0 and (b) D curves for $PI = 15$ % and $\sigma'_m = 200\ kPa$ compared with experimental data in the range of $10\% < PI < 20\%$ and $100\ kPa < \sigma'_m < 300\ kPa$.

At this point, two critical issues must be clarified. The first one is that equations (21) and (22) give only an estimation of the dispersion affecting the curves. Indeed, the adopted procedure does not propagate in a rigorous manner the uncertainties of the multiple variables related to the nonlinear relationships. Therefore, care should be exercised when equations (21) and (22) are used for practical applications. The development of a predictive model to be used for probabilistic analyses is beyond the scope of this study.

The second issue is that the relationships were developed on the basis of experimental tests carried out at σ'_m ranging from 30 to 440 kPa on soils characterized by PI ranging from 0 to 42 %. Moreover, data refer to tests where a maximum γ_c amplitude equals to 1 % was reached. The relationships cannot then be used outside these limits because no experimental data were used to constraints the predictive model outside these ranges.

6. Conclusions

The dynamic behaviour of silty and clayey soils from Central Italy was studied by means of cyclic laboratory tests for the seismic microzonation of several municipalities damaged by the 2016-2017 seismic sequence. The analysis of the database, which includes almost 80 tests, led to the following observations:

1) The trends observed in the comparison between field and laboratory V_S values confirm previous studies, with a marked difference especially for stiff soils. On the other side, for highly deformable soils the reconsolidation process may have played a crucial role, inducing the overestimation of $V_{S,lab}$ with respect to $V_{S,field}$.
2) The volumetric shear strain threshold γ_{tp}, as estimated from the cyclic pore-water pressure generation can be considered an index of the reliability of laboratory tests. Indeed the comparison with conventional estimates revealed the presence of outliers which are associated to unreliable results. Further investigations are needed to fully understand the causes of these discrepancies.
3) The investigated soils exhibit larger values of the linear thresholds than those reported in the literature, but comparable values of the volumetric threshold strain. Moreover, the linear threshold shows an increasing dispersion with increasing PI. Care should then be exercised when predictive models are used for soils characterized by high PI values.
4) An increase in the small strain damping ratio D_{min} is observed with increasing PI and f. As a consequence, an overestimation of D_{min} was observed in results from RC tests, compared to the corresponding values from TS tests. A normalization procedure was then proposed to correct values of D_{min} from RC tests to a f equals to 1 Hz. Further specific studies about the influence of f on RC results are needed to generalize the proposed procedure.

The database has been then used to calibrate the Darendeli (2001) predictive model for typical Central Italy soils. The updated model is able to capture the peculiarities of the nonlinear behaviour within the investigated ranges of PI, σ'_m, and γ_c. The predictive relationships revealed a broad range of the $G_S/G_0 - \gamma_c$ curves with increasing PI and, on the contrary, a narrow range of G_S/G_0 and D with increasing σ'_m, suggesting a less marked effect of σ'_m than in Darendeli study. The updated model represents a useful tool to model fine-grained soils in site response analyses for Central Italy sites.

Acknowledgements

The project was carried out with the funding from Italian Government within the Level 3 Seismic Microzonation of 138 municipalities severely shaken by the Central Italy earthquakes. This funding is gratefully acknowledged. The Seismic Microzonation Center ("*Centro per la Microzonazione Sismica e le sue Applicazioni*"), entrusted with the task of providing scientific support and coordination of the activities, is also gratefully acknowledged.

The Authors want to thank all the people who contributed in the execution of the laboratory tests: Silvano Silvani and Marco Bonaventura (Sapienza Università di Roma), Oronzo Pallara, Giovanni Bianchi, Viviana Chetry and Irene Coppetta (Politecnico di Torino), Antonio Cammarota and Alfredo Ponzo (Università di Napoli Federico II), Valeria Bandini and Giuseppe Di Filippo (Università di Messina), Eusebio Castellano and Francesco Contino (Università Kore di Enna).

7. References

Akeju OV, Senetakis K, Wang Y (2017) Bayesian Parameter Identification and Model Selection for Normalized Modulus Reduction Curves of Soils. Journal of Earthquake Engineering:1-29

Anderson DG, Woods RD Comparison of field and laboratory shear moduli. In: In Situ Measurement of Soil Properties, Raleigh, N.C., 1975. ASCE, pp 66-92

ASTM International (2011) ASTM D2487-11 Standard practice for classification of soils for engineering purposes (Unified Soil Classification System). ASTM International, West Conshohocken

Bjerrum L, Landva A (1966) Direct simple-shear tests on a Norwegian quick clay. Geotechnique 16:1-20

Caielli G, De Franco R, Di Fiore V, Albarello D, Amanti M, et al. (2019) Extensive geophysical prospecting for seismic microzonation. Bulletin of Earthquake Engineering This Issue

Cascante G, Vanderkooy J, Chung W (2003) Difference between current and voltage measurements in resonant-column testing. Canadian Geotechnical Journal 40:806-820

Ciancimino A et al. (2019) Dynamic characterization of fine-grained soils for the seismic microzonation of Central Italy. Paper presented at the 7th International Conference on Earthquake Geotechnical Engineering, Rome, 17-20 June

d'Onofrio A, Silvestri F, Vinale F (1999) Strain rate dependent behaviour of a natural stiff clay. Soils and Foundations 39:69-82

D'Elia B, Lanzo G, Pagliaroli A Small-strain stiffness and damping of soils in a direct simple shear device. In: Engineering NZSfE (ed) Pacific conference on earthquake engineering, Christchurch, New Zealand, 2003.

Darendeli MB (2001) Development of a new family of normalized modulus reduction and material damping curves. PhD Dissertation, University of Texas at Austin

Dobry R, Ladd R, Yokel FY, Chung RM, Powell D (1982) Prediction of pore water pressure buildup and liquefaction of sands during earthquakes by the cyclic strain method. vol 138. National Bureau of Standards Gaithersburg, MD,

Dobry R, Vucetic M (1987) Dynamic properties and seismic response of soft clay deposits.

Doroudian M, Vucetic M (1995) A direct simple shear device for measuring small-strain behavior. Geotechnical Testing Journal 18:69-85
Doroudian M, Vucetic M Small-strain testing in an NGI-type direct simple shear device. In: Proc. 11th Danube-European Conf. on Soil Mechanics and Geotech. Engrg., Porec, Croatia, AA Balkema, 1998. pp 687-693
EPRI (1993) Modeling of dynamic soil properties. Palo Alto, California
Hardin BO, Drnevich VP (1972) Shear modulus and damping in soils: design equations and curves. Journal of Soil Mechanics & Foundations Div 98:667-692
Hwang SK (1997) Dynamic properties of natural soils. PhD Dissertation, University of Texas at Austin
Isenhower WM (1979) Torsional simple shear/resonant column properties of San Francisco Bay mud. University of Texas at Austin
Isenhower WM, Stokoe K (1981) Strain-rate dependent shear modulus of San Francisco Bay mud. Paper presented at the Int Conf on Recent Advances in Geotechnical Earthquake Engineering and Soil Dynamics, St. Louis, Missouri,
Ishibashi I, Zhang X (1993) Unified dynamic shear moduli and damping ratios of sand and clay. Soils and Foundations 33:182-191
Kim DS (1991) Deformational characteristics of soils at small to intermediate strains from cyclic test. PhD dissertation, University of Texas at Austin
Kishida T (2016) Comparison and correction of modulus reduction models for clays and silts. Journal of Geotechnical and Geoenvironmental Engineering 143:04016110
Kokusho T, Yoshida Y, Esashi Y (1982) Dynamic properties of soft clay for wide strain range. Soils and Foundations 22:1-18
Lanzo G, Doroudian M, Vucetic M Small-strain cyclic behavior of Augusta clay in simple shear. In: Proc. of the 2nd Int. Symposium on Pre-failure Deformations Characteristics of Geomaterials, 1999. pp 213-220
Lanzo G, Vucetic M (1999) Effect of soil plasticity on damping ratio at small cyclic strains. Soils and Foundations 39:131-141
Lanzo G, Vucetic M, Doroudian M (1997) Reduction of shear modulus at small strains in simple shear. Journal of Geotechnical and Geoenvironmental Engineering 123:1035-1042
Lo Presti DC Proprietà dinamiche dei terreni. In: XIV CGT, Torino, 1989. Politecnico di Torino, pp 1-62
Lo Presti DC Discussion on" threshold strain in Soils". In: X ECSMFE on Deformation of Soils and Displacements of Structures, Firenze, Italy, 1991. AA Balkema, pp 1282-1283
Lo Presti DC, Jamiolkowski M, Pallara O, Cavallaro A, Pedroni S (1997) Shear modulus and damping of soils. Geotechnique 47:603-617
Masing G Eigenspannumyen und verfeshungung beim messing. In: Proc. Inter. Congress for Applied Mechanics, 1926. pp 332-335
Matešić L, Vucetic M (2003) Strain-rate effect on soil secant shear modulus at small cyclic strains. Journal of geotechnical and geoenvironmental engineering 129:536-549
Meng J, Rix G (2003) Reduction of equipment-generated damping in resonant column measurements. Géotechnique 53:503-512
Mortezaie A, Vucetic M (2016) Threshold shear strains for cyclic degradation and cyclic pore water pressure generation in two clays. Journal of Geotechnical and Geoenvironmental Engineering 142:04016007
Régnier J et al. (2018) PRENOLIN: International benchmark on 1D nonlinear site-response analysis—Validation phase exercise. Bulletin of the Seismological Society of America 108:876-900
Seed H, Idriss I (1970) Soil moduli and damping factors for dynamic response analyses, Report no. EERC 70-10. Earthquake Engineering Research Center, University of California, Berkeley, California
Senetakis K, Anastasiadis A, Pitilakis K (2015) A comparison of material damping measurements in resonant column using the steady-state and free-vibration decay methods. Soil Dynamics and Earthquake Engineering 74:10-13
Shibuya S, Mitachi T, Fukuda F, Degoshi T (1995) Strain rate effects on shear modulus and damping of normally consolidated clay. Geotechnical testing journal 18:365-375
Silver ML, Seed HB (1971) Volume changes in sands during cyclic loading. Journal of Soil Mechanics & Foundations Div
Stewart JP (2008) Benchmarking of nonlinear geotechnical ground response analysis procedures. Pacific Earthquake Engineering Research Center,
Stewart JP, Afshari K, Hashash YM (2014) Guidelines for performing hazard-consistent one-dimensional ground response analysis for ground motion prediction. PEER Report 2014 16
Stokoe K, Darendeli M, Andrus R, Brown L Dynamic soil properties: laboratory, field and correlation studies. In: Proc. 2nd Int. Conf. Earthquake Geotech. Engg, 1999. pp 811-846
Stokoe K, Hwang S, Lee J-K, Andrus RD Effects of various parameters on the stiffness and damping of soils at small to medium strains. In: PRE-FAILURE DEFORMATION OF GEOMATERIALS. PROCEEDINGS OF THE INTERNATIONAL SYMPOSIUM, 12-14 SEPTEMBER 1994, SAPPORO, JAPAN. 2 VOLS, 1995.
Stokoe K, Santamarina JC Seismic-wave-based testing in geotechnical engineering. In: ISRM International Symposium, 2000. International Society for Rock Mechanics,

Stoll RD, Kald L (1977) Threshold of dilation under cyclic loading. Journal of the Geotechnical Engineering Division 103:1174-1178
Tabata K, Vucetic M Threshold shear strain for cyclic degradation of three clays. In: 5th Int. Conf. on Recent Advances in Geotechnical Earthquake Engineering and Soil Dynamics, Missouri Univ. of Science and Technology, San Diego, May 24th - May 29th 2010.
Vardanega P, Bolton M (2013) Stiffness of clays and silts: Normalizing shear modulus and shear strain. Journal of Geotechnical and Geoenvironmental Engineering 139:1575-1589
Vucetic M Soil properties and seismic response. In: Proc. 10th World Conference on Earthquake Engineering, 1992. pp 1199-1204
Vucetic M (1994) Cyclic threshold shear strains in soils. Journal of Geotechnical engineering 120:2208-2228
Vucetic M, Dobry R (1991) Effect of soil plasticity on cyclic response. Journal of geotechnical engineering 117:89-107
Wang Y-H, Cascante G, Santamarina JC (2003) Resonant column testing: the inherent counter emf effect. Geotechnical Testing Journal 26:342-352
Youd TL (1972) Compaction of sands by repeated shear straining. Journal of Soil Mechanics & Foundations Div 98
Zalachoris G, Rathje EM (2015) Evaluation of one-dimensional site response techniques using borehole arrays. Journal of Geotechnical and Geoenvironmental Engineering 141:04015053
Zhang J, Andrus RD, Juang CH (2005) Normalized shear modulus and material damping ratio relationships. Journal of Geotechnical and Geoenvironmental Engineering 131:453-464